Agricultural Water Management 307 (2025) 109257

Contents lists available at ScienceDirect

Agricultural Water Management

journal homepage: www.elsevier.com/locate/agwat

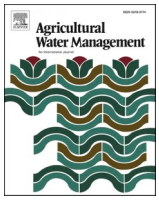

Dynamics and associations of selected agrometeorological variables in Robusta growing regions of Uganda

Ronald Ssembajwe [a,b], Catherine Mulinde [a], Saul D. Ddumba [a], Godfrey H. Kagezi [b], Ronald Opio [a], Judith Kobusinge [b], Frank Mugagga [a], Yazidi Bamutaze [a], Anthony Gidudu [c], Geoffrey Arinaitwe [b], Mihai Voda [d,*]

[a] College of Agricultural and Environmental Sciences, Makerere University, P.O. Box 7062 University Rd, Kampala, Uganda
[b] National Coffee Research Institute, National Agricultural Research Organization, P.O. Box 185, Mukono, Uganda
[c] College of Engineering, Design Art and Technology, Makerere University, P.O. Box 7062 University Rd, Kampala, Uganda
[d] Faculty of Geography, Dimitrie Cantemir University, Bodoni Sándor Street 3–5, Târgu Mureș, Romania

ARTICLE INFO

Handling Editor - Dr Z Xiying

Keywords:
Agrometeorological variables
Trends
Associations
Robusta coffee
Productivity
Climate change

ABSTRACT

As climate variability increases with extremes becoming more frequent, the pressure on agriculture only intensifies. A better understanding of the dynamics of direct climate drivers of agricultural productivity is therefore sought. This study aimed to analyze the long-term and recent spatiotemporal trends and associations of selected agrometeorological variables in Robusta Coffee growing regions (RCGR) of Uganda for the period 1980–2021. We employed novel trend test and signal decomposition methods along with machine learning and correlation methods. Results show significantly increasing trends in monthly Vapor Pressure Deficit (VPD) in Amolatar, Kabale and Mbale while, Arua, Kituza and Masindi had decreasing trends. Additionally, significantly decreasing trends in Fraction of Absorbed Photosynthetically Active Radiation (FAPAR) except for Masindi, Abim and Amolatar districts in Kyoga basin were observed. However, there were generally no trends in Climate Water Balance (CWB) and Actual Evapotranspiration (AET) over the study region at 5 % level of significance. BEAST results revealed significant changes in Mbale's seasonal AET, abrupt changes in both trends and seasons of Kituza AET since 1982 with 10 % chances of occurrence, trend anomalies in Amolatar VPD since 2009. Furthermore, significantly decreasing and increasing trends in Potential Evapotranspiration (PET) and NPP respectively were observed across 70 % of the RCGR. El-Nino/Southern Oscillations accounted for only 2.5 % of the variance in PET. Strong negative and positive associations were observed between PET and NPP in the Northern sub region and Mid-Eastern stretch respectively. Therefore, urgent interventions in form of seasonal schedule restructuring and optimal irrigation use and management to increase productivity especially in areas where CWB is below 0 for over 3 months, offset the increasing VPD and as well effectively manage pest and diseases are recommended.

1. Introduction

Agrometeorological variables such as Evapotranspiration (ET), Vapor Pressure Deficit (VPD), Fraction of Absorbed Photosynthetically Active Radiation (FAPAR) and Climate Water Balance (CWB) play a vital role in determining crop suitability, precise management and, designing sustainable climate adaptation schemes over a given region (Pereira et al., 2011; Anapalli et al., 2020; Kiran et al., 2020; Montazar et al., 2020). Understanding the nature and dynamics of these Essential Climate Variables (ECV) (Bojinski et al., 2014) is therefore key to informing viable adaptation and mitigation strategies especially in Agro-based economies like Uganda where, 70 % of the working population is employed in agriculture (UBOS, 2018; World Bank, 2018). According to Sankaran et al. (2020), any improved understanding on the fluctuations and scaling characteristics of such time series may enhance the modeling efforts aimed at a fuller understanding of their structures and, accurate prediction of their courses in the future especially in Robusta Coffee Growing Regions (RCGR) of Uganda.

Uganda is the birth place of Robusta coffee and the leading producer of the species contributing up to 30 % of the total global Robusta coffee market share (Patform, 2019). These Robusta coffee varieties contribute 80 % of the country's total coffee exports with an estimated productivity

* Corresponding author.
E-mail address: mmvoda@yahoo.com (M. Voda).

https://doi.org/10.1016/j.agwat.2024.109257
Received 19 September 2023; Received in revised form 14 December 2024; Accepted 16 December 2024
Available online 22 December 2024

of 4 kg/tree (UCDA, 2022). This is however way below the optimal productivity of the crop in comparison with 10 kg/tree (Platform, 2019; Helena Coffee, 2022) from other Robusta producing countries such as Vietnam, Brazil, Columbia among others. This low productivity is attributed to emergence of new pests and diseases (Kansiime et al., 2017), low adoption of good agronomic practices (Kagezi et al., 2017, 2020), declining soil fertility (Musoli, 2001, 2016), extreme environmental conditions all being derivatives of climate variation and change (DaMatta et al., 2018). Additionally, climate as an agricultural production factor has a pivotal role in regulating important aspects of coffee ecosystems including the plants' phenology (Kouadio et al., 2021), soil moisture availability, pest population and disease dynamics (Kagezi et al., 2017) among others. Understanding the nature of this complex interaction requires an interdisciplinary approach to identify critical components needed to develop management tools to address the poor growth, pest and disease concerns of a farmer (Olatinwo et al., 2013). This necessitates a thorough assessment of climate variables able pin point and explain this complex crop-climate interaction.

Previous studies in Uganda led by Basalirwa (1995); Phillips and Mcintyre (2000); Funk et al. (2012); Nimusiima et al. (2013); Nsubuga et al. (2014); Majaliwa et al. (2015); Mubiru et al. (2018) Gebrechorkos et al. (2019); Obubu et al. (2021) among others have largely concentrated on understanding the dynamics of selected climate variables such as precipitation and temperature whose results have had limited applications in crop production especially for coffee because they can't fully explain the variations in the crop's productivity (Thornthwaite and Mather, 1955; Black et al., 2016; Asfaw et al., 2018), resurgence and emergency of new pests and diseases (Kansiime et al., 2017). The few studies that have taken an extra step to include Potential Evapotranspiration (PET/ ET_o) include Mubialiwo et al. (2020) over the Mpologoma Catchment East of the RCGR and Onyutha et al. (2021) over the four water management zones in Uganda. Both studies adopted the Hargreaves method (Hargreaves and Samani, 1985) whose applications are limited to non-humid regions of the world (Jensen et al., 1990; Trajkovic, 2007) with over and underestimations of inland and onshore ET_o respectively (Bautista et al., 2009; Berti et al., 2014). The method is also known for its weakness in deriving PET on timescales less than five days (Berti et al., 2014) which the later study considered in the preliminary computation of PET. These weaknesses were apparent in the findings of Onyutha et al. (2021) as PET magnitudes over Lake Victoria were significantly low (<1000 mm) compared to magnitudes over the remaining lakes (>3500 mm) and most parts of the country. More so, these studies were performed at low temporal and spatial resolutions of 0.5° x 0.5° and 0.25° x 0.25° grids and Annual temporal scales necessitating the adoption of high-resolution agrometeorological data.

The agrometeorological variables adopted in this study have been broadly studied to have a direct influence on the productivity of the plant and the interactions in the entire ecosystem. For example, Feddema, (2005) noted that PET represents the potential water use by an ecosystem, and, as such, is a measure of potential plant productivity. Furthermore, physical and physiological processes in plants are controlled by observable attributes, such as the leaf area index (LAI), soil moisture or evapotranspiration (Landsberg and Gower,1997; Zakeri and Mariethoz, (2021). Additionally, water stress and or deficit owing to increasing evaporative demand or vapor pressure deficit decreases photosynthesis and the supply of photosynthate consequently affecting the plant's productivity (World Meteorological Organization, 2012; Amitrano et al., 2021). Several other studies including Stegman, (1988); Gutierrez and Meinzer, (1994); Ministry of Agriculture, (2001); Hunsaker et al. (2003); Pereira et al. (2011); Wratt et al. (2006); Droogers et al. (2012); Mulovhedzi et al. (2020); Kumar et al. (2020); Santos et al. (2020); Anapalli et al. (2020); Kiran et al. (2020); Montazar et al. (2020) among others have underscored the added-value of more direct agrometeorological variables such as FAPAR, ET, CWB and VPD in defining both plant health, productivity and their ecosystems interaction. However, despite their importance, a few studies in Uganda especially Robusta coffee growing regions (RCGR) have embarked on understanding their trends and variability.

The availability of remotely sensed data for observing Earth's climate and atmosphere is growing rapidly presenting an opportunity for researchers to further explore and quantify the effect of the previously unexplored but essential agrometeorological variables at high resolutions even in remote areas (Anderson et al., 2016; Voda et al., 2018; Devasthale and Carlund, 2022). This study adopted the remotely sensed Net Primary Productivity (NPP) as a proxy for coffee yield in the study region in accordance with Li and Tan (2014) study recommendations for its high spatial resolution attribute and for the fact that quality long-term coffee yield data was not available at the time of this study. The relationship between yield and NPP is scientifically established by Prince et al. (2001) and, conventionally, various studies have employed regression, process-based models and crop inventory-based estimates to derive NPP from crop yield data. A detailed description of such approaches have been given in Bolinder et al. (2007). It was emphasized by Cao et al. (2022) that finer-scale analysis of the spatial pattern of changes in crop yield variability is crucial to gain a better understanding of the spatial heterogeneity of food production capacity in response to climate change. Mariethoz et al. (2012) explored the ability of geostatistical simulation methods to characterize spatiotemporally varying fields such as evapotranspiration, rainfall, and temperature (Zakeri and Mariethoz, 2021). The objectives of this study therefore were to; (i) describe the recent and long-term temporal and spatial trends in the VPD, AET, FAPAR, CWB and PET in the Robusta Growing Regions of Uganda; (ii) examine the change points, seasonal variability and spatiotemporal covariance of AET, VPD and PET in the RCGR respectively and, (iii) determine associations between PET and NPP in RCGR of Uganda for the period 1980–2021 using a suite of station and satellite observed climate and agroclimatic data so as to inform feasible management and adaptation measures to climate change.

2. Description of study area

This study was done in the Five major coffee growing regions of Uganda (Wang et al., 2015) a developing tropical country found in East Africa and situated within 1°S-5°N and 29°E-36°E (Basalirwa, 1995; Bakamanume, 2010 and Mugume, 2018) that include the Western Highlands, Elgon sub-region, West Nile stretch and areas around Lake Victoria And Kyoga basins (Fig. 1).(Fig. 2 and Fig. 3) V

These regions boost over 1.7 million households (UCDA, 2022) involved either directly or indirectly in coffee production. The area is generally low lying in the L.Victoria and Kyoga basins with a gradual slope reducing towards the West Nile stretch with an average altitude of 1100 m and 900 m respective. While as, the Western and southwestern of Mt.Rwenzori slopes, Kigezi sub-region, Isingiro, Mt Elgon sub-region are generally mountainous with average altitude of 1800 m and above (Stanton et al., 2017). The region largely enjoys an equatorial type of climate with two distinct(bimodal) wet seasons in the Eastern, Western and Central parts between February and May and September to December while the Northern sub region has unimodal rainfall season mainly concentrated in between April and July. The annual rainfall ranges from more than 2000 mm on the shores of L. Victoria and the high terrain to less than 100 mm over north east part of Uganda, Karamoja. The main rains are received between March and June, and rainfall totals of more than 500 millimeters (mm) during this season typically provide enough water for crops and live- stock (Funk et al., 2012).(Table 1)

3. Data and methods

3.1. Data sources and pre-processing

This study considered a suite of Observed rainfall, max and min air temperature, Relative humidity and Evapotranspiration data obtained

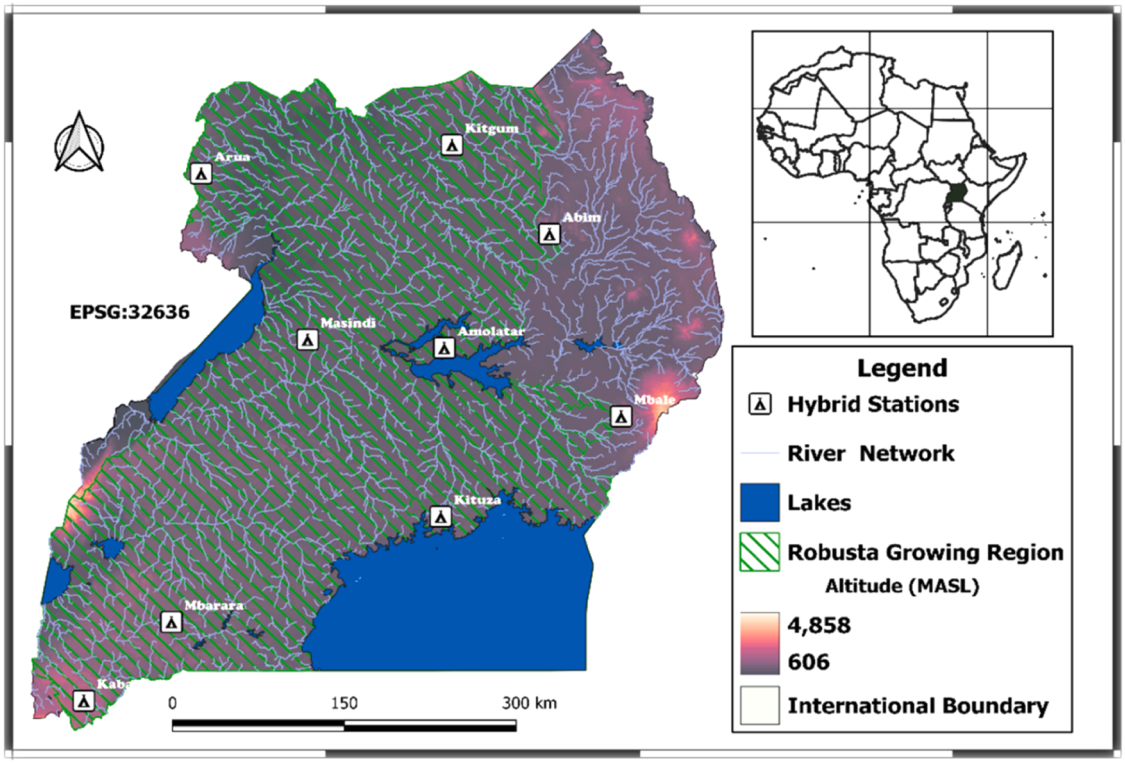

Fig. 1. Robusta coffee growing regions of Uganda as stipulated in UCDA Robusta Handbook.

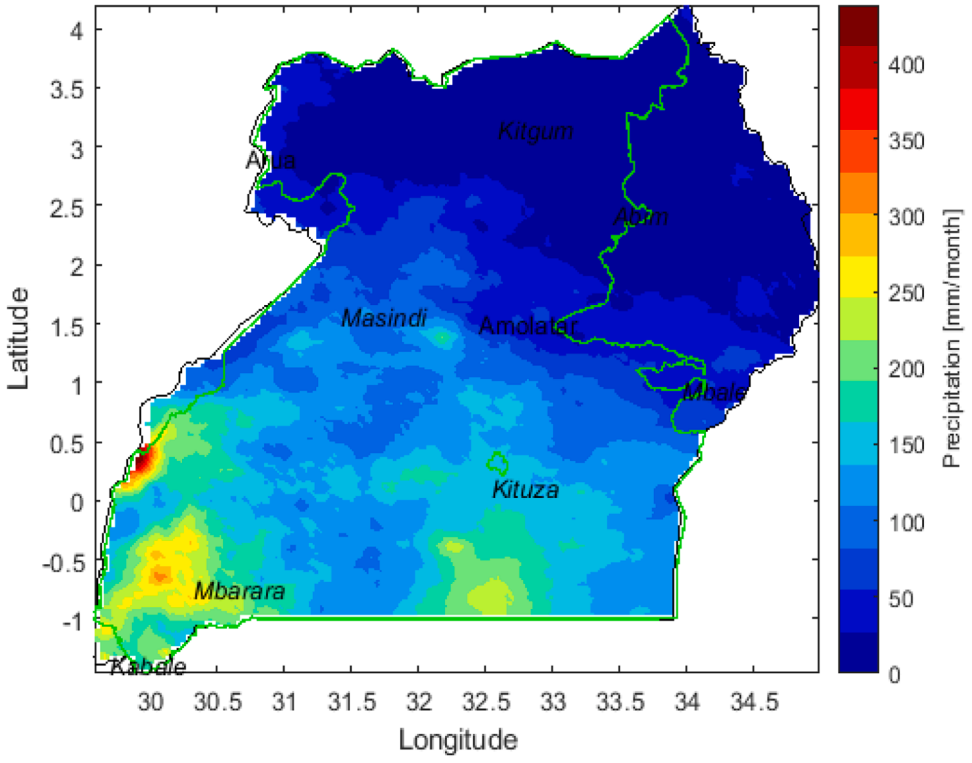

Fig. 2. Monthly Precipitation Climatology of Uganda (1983–2021) computed from TAMSAT V3.1 data and Station data. The RCGR is shown by the lime-green boundary.

from the Uganda National Meteorological Authority (UNMA) for 9 selected hybrid stations covering the five major coffee growing regions of Uganda at monthly scales for the period 1980–2021, and TAMSAT (2022) Satellite estimates of rainfall (Maidment et al., 2017) at a 0.043° grid resolution to cater for the inadequacy of ground based observations in Uganda (Maidment et al., 2013). Vapor pressure deficit (VPD) data for a period 1980–2021 was computed as a difference between the saturated vapor pressure (e_{sat}) and the actual vapor pressure (e_{act}) as follows;

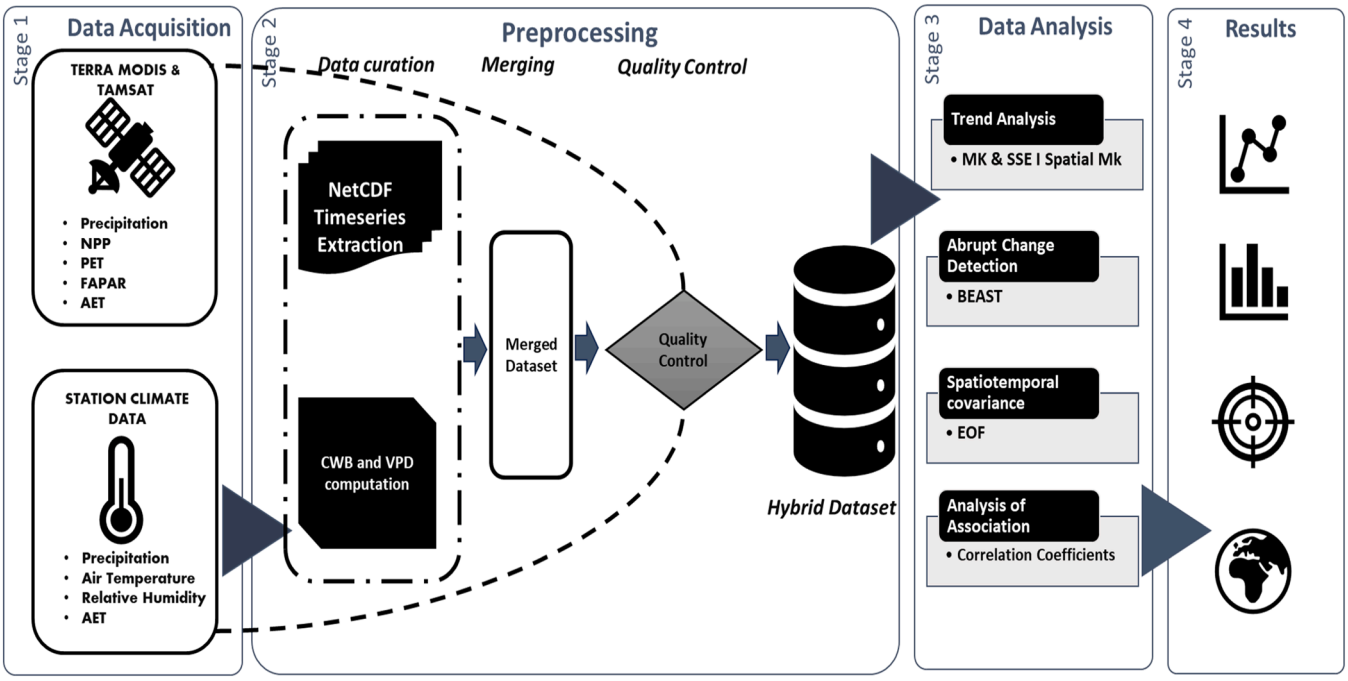

Fig. 3. Schematic overview of methodology, using both in situ observed and satellite derived climate and vegetation data from UNMA and, NASA and TAMSAT.

Table 1
Data and Sources.

Agromet Variable	Temporal	Spatial	Period	Notes	Source
VPD	Monthly	_____	1980–2021	Computed from station Air Temperature and Humidity data	(Uganda National Meteorological Authority, 2022)
FAPAR	8-Daily and Annual	500 Meters	2000–2021	Preprocessed	(NASA, 2022)
AET	Monthly and Annual	4 km Meters	1980–2021	Preprocessed	(Abatzoglou et al., 2018)
PET	8-daily and Annual	500 Meters	1980–2021	Preprocessed	(NASA, 2022) (Abatzoglou et al., 2018)
CWB	Monthly	_____	1980–2021	Computed from monthly Rainfall and Actual Evapotranspiration data	Uganda National Meteorological Authority, (2022)) (Maidment et al., 2017) (Abatzoglou et al., 2018)
NPP	Annual	500 Meters	2001–2021	Preprocessed	(NASA, (2022)

$$e_{sat} = 0.611 * \exp\left(\frac{17.502T}{T + 240.97}\right), \quad (1)$$

$$e_{act} = \quad e_{sat}\frac{RH}{100}, \quad (2)$$

$$; -VPD = e_{sat} - e_{act}, \quad (3)$$

where, (e_{sat}) is the saturated vapor pressure deficit (kPa); (e_{act}) is the actual vapor pressure (kPa); VPD is the vapor pressure deficit (kPa); T is mean air temperature in degrees Celsius and RH is relative humidity in percentage using both in situ observed and satellite derived climate data. The Climate Water Balance (CWB) was computed as a difference of monthly precipitation and actual evapotranspiration. Furthermore, Moderate resolution Imaging Spectrometer (MODIS) (Running et al., 2017) MODIS/TERRA derived Fraction of Absorbed Photosynthetically Active Radiation (FAPAR), Reference/Potential evapotranspiration (ETo/PET), Actual Evapotranspiration (Eta/AET) and Net Primary Productivity (NPP) data at 8-daily, monthly and annual temporal and 500 m spatial resolution for the study period was obtained from NASA, (2022). The Evapotranspiration products are NASA level 4 (highest quality controlled and validated) products based on daily meteorological forcing and remotely sensed vegetation dynamics using the Pennman-montieth equation (Running et al., 2017; Gaona et al., 2022). Satellite data was obtained in Network Common Data Form (NetCDF) format and data preprocessing for Uganda administration vector and timeseries extraction was done using the Mapping Toolbox in MATLAB R2019a software (The MathWorks Inc., 2019)

3.2. Quality control

The data was quality controlled by first checking for completeness in station meteorological data. Any missing data was then filled using the normal ratio method as recommended by Villazón and Willems, (2010). After filling the missing data, the data was tested for homogeneity using the double-mass curve for ground observed data in line with WMO, (2017) recommendation due to possible changes in the instrumentation and siting of stations (Mugume, 2018). Finally, The Root Mean Square Error (RMSE) (Chai and Draxler, 2014; Yang et al., 2014) was used to test the goodness of fit of hybrid estimates from both in situ and satellite data. TAMSAT 3.1 satellite data was used in accordance with study recommendations by Maidment et al. (2013). Quality Control results are summarized in the appendix.

3.3. Mann Kendall Trend test and Sen's slope estimator

In order to analyze long-term temporal and spatial trends, the modified Mann Kendall Trend test and Sen's slope estimator (MKSSE) was used. Mann Kendall test is a statistical test widely used for the analysis of trend in climatologic and in thermal and hydrometeorological time series (Yue and Wang, 2004) such as temperature, rainfall, evaporation, evapotranspiration, streamflow and water quality (Alashan, 2020). There are two advantages of using this test. First, it is a non-parametric test and does not require the data to be normally distributed. Second, the test has low sensitivity to abrupt breaks due to inhomogeneous time series (Tabari et al., 2011). Any data reported as non-detects are included by assigning them a common value that is smaller than the smallest measured value in the data set. According to this test, the null hypothesis H_o assumes that there is no trend (the data is independent and randomly ordered) and this is tested against the alternative hypothesis H_1, which assumes that there is a trend (Onoz et al., 2012). The computational procedure for the Mann Kendall test can be found in Drápela and Drápelová, (2011).

In the Mann-Kendall test, the null hypotheses were tested at 95% confidence level for Actual Evapotranspiration, Fraction of Absorbed Photosynthetically Active Radiation, Climate Water Balance, Vapor Pressure deficit and Net Primary productivity trends and their respective magnitudes at monthly timescales.

(ii) Sen's Slope Estimator Test

The slope which depicts change per unit time in the time series is explained by the Sen's procedure in the case of a linear trend (Sen, 1968).The magnitude of the trend is estimated by Sen's slope estimator (Q_i).

$$Q_i = \frac{X_j - X_k}{\mathrm{j} - \mathrm{k}} \tag{4}$$

for I = 1, 2,…,N

Where, X_j and X_k are data values at times j and k (j > k) respectively. The median of these N values of Q_i is represented as Sen's estimator.

$$Q_{med} = Q_{\frac{N+1}{2}} \text{ if N is odd and } Q_{med} = \left[\frac{Q_{\frac{N}{2}} + Q_{\frac{N+2}{2}}}{2}\right] \tag{5}$$

if N is even. A positive Q_i indicates an increasing trend and a negative value of Q_i shows a decreasing trend in the time series.

3.4. Bayesian estimator for abrupt changes in seasons and trends (BEAST)

BEAST is a generic Bayesian time-series decomposition algorithm for changepoint detection and nonlinear trend analysis (Zhao et al., 2019). Change detection methods provide access to recovery trajectories of trend and seasonality and detect abrupt changes in time series (Fang et al., 2018; Li et al., 2022). From a mathematical perspective, the search for ecological interpretations of a time series reduces to finding the relationship between a given climate variable (y) and time (t) from the observed data at n points of time. $\mathcal{D} = \{t_i, y_i\}, i = 1,\ldots,n$, via a statistical decomposition model $\hat{y}(t) = f(t)$. The model generally treats the time series $\hat{y}(t_i)$ as an addition of seasonal S(•) and trend T(•) signals;

$$\hat{y}(t_i) = \mathrm{f}(t_i;\Theta_s) + \mathrm{T}(t_i;\Theta_T) \quad , \quad i = 1,\ldots,n, \tag{6}$$

where the parameters Θ_s and Θ_T specify the seasonal and trend signals; they also implicitly encode the abrupt changes. By analogy to linear regression, the time t and data y are independent and dependent variables, respectively; Θ_s and Θ_T are parameters to be estimated from the data $\mathcal{D}$ (Zhao et al., 2019). BEAST was used to demystify both short-term, long term and seasonal dynamics of trends the agrometeorological variables in MATLAB using the BEAST Toolbox (Gerber and Furrer, 2019).

3.5. Empirical orthogonal function (EOF) for spatiotemporal covariance analysis

The EOF technique is widely applied for examining of the spatial and temporal variability of large multidimensional datasets with a devoted use in meteorological studies (Lorenz, 1956; Dommenget and Latif, 2002;Yosef et al., 2017). It can be used to identify and separate the dominant and the underlying processes and essential parameters of a given use case for example major drivers of potential evapotranspiration patterns and its corresponding signals. Its main goal is to decompose the parameters of the local climate region, and present a few patterns for each variable. According to Yosef et al. (2017), in atmospheric research, the popular configuration of the raw data matrix is referred to as S-mode analysis and represents the pattern's location (EOF) and the time series of the patterns called principal component (PC). The matrix has the structure of *MxN*, where *M* is the space dimensions and *N* is the shared sampling dimension. Computation of EOFs involves removal of the mean from the measurements first; the covariance matrix **F** can then be constructed as

$$\boldsymbol{F} = \frac{1}{N}\boldsymbol{R}^T\boldsymbol{R}, \tag{7}$$

where $\boldsymbol{R}$ is the raw data matrix, $\boldsymbol{R}^T$ is the transpose matrix, and *N* is the number of samples. Then, reconstructing the raw data **R** with a new time series PC and the eigenvectors (EOF),

$\boldsymbol{R}(t,x) = \sum_{allEOFs} PC(t)EOF(x)$ The decomposed patterns are considered empirical models (EOFs), which are orthogonal to each other in space and in time (Mestas-Nuñez and Enfield, 1999; Yosef et al., 2017)

The fraction of each *kth* mode EOF_k accounts for a variance is

$$\delta_k = L_k \Big/ \sum_{i=1}^{n} L_i \quad x \quad 100 \tag{9}$$

where L is the eigenvalue value of the *kth* eigenvector EOF_k.

The computation of PET EOFs and associated PCs was done using the CDT Toolbox (Greene et al., 2019) in MATLAB.

3.6. Spatiotemporal correlation analysis

Correlation coefficients are widely used to measure association between variables measured across a set of spatial locations in time. Unlike the default Pearson's linear correlation coefficient, high-dimensional correlation analysis is a method for visualizing the relationships among the variables in multi-dimensional data and their temporal behavior by applying the complex cross-correlation function (Harrington et al., 2000). The approach has gained reference in hydrological research (Dikbaş, 2017) due to its ability to express both quantitatively and qualitatively the relationship between higher dimensional datasets as well as its strength over the linear correlation coefficient in estimating the anti-correlation (Sagehorn et al., 2023). Typically, the static component is removed before calculating the correlations (Harrington et al., 2000). In our case the averages of the PET and NPP with respect to time were considered good estimates for the static component. A detailed description of the computational procedure of the high dimension correlation coefficient can be found in Dikbaş, (2017), Mohapatra and Weisshaar, (2018) and Sagehorn et al., (2023). The high dimension correlation computation for this study was done in MATLAB using the spatial correlation function (Kumar, 2024).

All computing was performed using Python Version 3.10 (Van Rossum and Drake Jr, 2009) and MATLAB R2019a (The MathWorks Inc., 2019) software on an Intel i5 7th gen computer, with 32 GB RAM. The code employed was written according to the principles of research

transparency and reproducibility and relied heavily on the Pandas, Numpy, Matplotlib, Xarray, Cartopy and Pymannkendall libraries in Python and Mapping Tool box (Bevilacqua et al., 2018), CDT (Greene et al., 2019) and BEAST (Gerber and Furrer, 2019) Toolboxes in MATLAB.

4. Results

4.1. Long term summary statistics of monthly essential climate variables

Tables 2, 3 and 4 show summaries of descriptive statistics and MKSSE for AET, VPD, CWB for the period 1980–2021, and 8-daily FAPAR from 2000 to 2021.

Generally, the results show that the highest monthly mean AET for the RCGR was recorded in the Western Highlands, Lake Kyoga and Lake Victoria basins, that is in Masindi (98.4 mm), followed by Amolatar and Kituza (97 mm both), Mbale (96.6 mm), Arua (94.4 mm), Kitgum (88.3 mm), Abim (80.5 mm), Kabale (71.1 mm). The lowest AET was recorded at Mbarara (66.7) with the southwestern RCGR. AET (Fig. 4) in the Eastern-Central, Western-Central and Northern stations rises abruptly from a general average of 60 mm in February to 120 mm in March through April and May and drops to 100–90 mm in June-July before it rises to above 120 mm in October. Hence, the annual cycles of AET in these zones/regions approximately describes a flat M-shaped pattern. On the other hand, stations within the Lake Victoria basin such as Kabale, Mbarara and Kituza had annual AET cycles characterized by a similar bimodal sinusoidal pattern that peaks in the months of March-April and October and troughs in February and July with significantly different magnitudes. That's, the first peak is 113 mm (Kituza) and 82 mm (Kabale) in March and 88 mm (Mbarara) in April and the second peak is 110 mm (Kituza), 83 mm (Kabale) and 90 mm (Mbarara) in November, and the first trough is 80 mm (Kituza), 70 mm (Kabale), 50 mm (Mbarara) and the second 80 mm (Kituza), 40 mm (Kabale), 20 mm (Mbarara) in February and July respectively.

Similarly, CWB results show a general surplus of the monthly mean CWB for all stations however with high standard deviations of ± 66 mm (Mbale), ± 59 mm (Kituza), ± 53 mm (Arua), ± 48 mm (Kabale), ± 46 mm (Amolatar), ± 42 mm (Kitgum and Masindi), ± 41 mm (Abim) and ± 26 mm (Mbarara).

On the other hand, the highest monthly mean VPD was observed at Kitgum (1.42kPa) and Abim (1.26kPa) followed by Arua (1.15kPa) Amolatar (1.13kPa), while Kituza (0.66kPa), Mbale (0.57kPa), Masindi (0.56kPa), Mbarara (0.32kPa) and Kabale (0.42) had the least. The Annual cycle of VPD (Fig. 5) in the RCGR follows a similar U-shaped pattern except for Kituza, Kabale and Mbarara stations. That's, peaks in February and gradually reduces to a minima in July then starts rising in August up-to January. Alternatively, Mbarara and Kabale stations in the southern region are characterized by a bimodal pattern with peaks in February and July. Kituza station VPD on the other hand is characterized by a distinct stable pattern with little interannual variability (± 0.2kPa SD) while the highest interannual variability is observed in Kitgum with a range of (<0.9 - >2.3kPa). The highest per-month mean VPD (2.3kPa) in the RCGR is recorded at the Northern (Kitgum) station in February while the lowest (0.32kPa) is recorded at the Southern (Kabale) station in April.

8-daily FAPAR results show that Lake Victoria basin and Elgon sub-region had the highest averages of 0.58 and 0.57 in Kituza and Mbale, respectively; followed by 0.56 in the Western highlands of Masindi. FAPAR averages over the Lake Kyoga basin for Abim and Amolatar were 0.50 and 0.45, respectively. Lowest 8-daily FAPAR averages were again observed in Kable (southwestern RCGR) at 0.40. The FAPAR annual cycles (Fig. 6) for the selected stations in the RCGR differed both slightly and greatly at different stations for the period 2000–2021. For example, Masindi, Amolatar and Mbarara follow similar bimodal patterns that peak in May and November differentiated by only magnitudes. Of the three, Masindi has the highest followed by Amolatar and lastly Mbarara.

Table 2
Summary of results on Descriptive and MKSSE of agrometeorological variables for Abim, Amolator and Arua stations.

	Abim						Amolatar						Arua					
Variable	Mean	SD	Min	Max	Z-Value	Slope	Trend	Mean	SD	Min	Max	Z-Value	Slope	Trend	Mean	SD	Min	Max	Z-Value	Slope	Trend
AET	80.5	40.1	1.9	146	0.202	0.002	No Trend	97	34.8	3	150	1.121	0.008	No Trend	94.4	36.2	5.6	148	−2.5	−0.02	Decreasing
VPD	1.26	0.41	0.48	2.78	1.706	0.0002	No Trend	1.13	0.38	0.45	3.79	3.81	0.0004	Increasing**	1.15	0.36	0.6	2.25	−5.96	0.0006	Decreasing**
FAPAR	0.5	0.2	0.04	0.95	1.67	3.45	No Trend	0.45	0.11	0.06	0.93	0.55	0.0	No Trend	——	——	——	——	——	——	——
CWB	10.4	41.3	−71	346	0.4	0.001	No Trend	12.5	45.5	−76.2	316	0.66	0.004	No Trend	20.3	53.4	−70.7	337	−0.875	−0.0066	No Trend

Note: H_o rejected when P<0.05 and, * ⇔ P < 0.01, * * ⇔ P < 0.001, * ** ⇔ P < 0.0001

Table 3
Summary of results on Descriptive and MKSSE of agrometeorological variables for Kabale, Kitgum and Kituza Stations.

	Kabale							Kitgum							Kituza						
Variable	**Mean**	**SD**	**Min**	**Max**	**Z-Value**	**Slope**	**Trend**	**Mean**	**SD**	**Min**	**Max**	**Z-Value**	**Slope**	**Trend**	**Mean**	**SD**	**Min**	**Max**	**Z-Value**	**Slope**	**Trend**
AET	71.8	20.3	6.5	102	−1.102	0.005	No Trend	88.3	43	1.8	157	−0.543	−0.005	No Trend	97	21	13	138	0.44	0.002	No Trend
VPD	0.45	0.1	0.24	0.82	5.07	0.0002	Increasing* **	1.42	0.5	0.56	3.38	1.35	0.0002	No Trend	0.64	0.15	0.31	1.55	−2.12	−0.00001	Decreasing
FAPAR	0.4	0.15	0.04	1	−2.497	−3.623	Decreasing	———	———	———	———	———	———	———	0.58	0.21	0.04	1	−2.76	−6.163	Decreasing*
CWB	17.2	48	−57.6	534	−0.53	−0.005	No Trend	11	42	−74	331	0.47	0.002	No Trend	23.4	58.8	−83	484	1.144	0.013	No Trend

Note: H_o rejected when $P < 0.05$ and, * ⇔ $P < 0.01$, * * ⇔ $P < 0.001$, * ** ⇔ $P < 0.0001$

Table 4
Summary of results on Descriptive and MKSSE of agrometeorological variables for Masindi, Mbale and Mbarara stations.

	Masindi							Mbale							Mbarara						
Variable	**Mean**	**SD**	**Min**	**Max**	**Z-Value**	**Slope**	**Trend**	**Mean**	**SD**	**Min**	**Max**	**Z-Value**	**Slope**	**Trend**	**Mean**	**SD**	**Min**	**Max**	**Z-Value**	**Slope**	**Trend**
AET	98.5	31	3.6	143	0.758	0.006	No Trend	96.6	24.9	9	147	−0.506	−0.003	No Trend	66.7	34	0.3	123	−0.388	−0.004	No Trend
VPD	1	0.3	0.55	2.13	−2.17	−0.0002	Decreasing	0.91	0.26	0.48	2.34	2.72	0.0002	Increasing*	0.8	0.16	0.25	1.3	2.1	0.0001	Increasing
FAPAR	0.56	0.17	0.04	1	−1.89	−3.33	No Trend	0.57	0.13	0.08	0.91	−2.99	−3.43	Decreasing*	0.32	0.101	0.02	0.64	−15.204	−0.002	Decreasing* **
CWB	10.35	41.7	−88	235	0.61	0.004	No Trend	24.7	66.3	−81	504	1.236	0.015	No Trend	5.4	26	−52	260	0.344	0.0005	No Trend

Note: H_o rejected when $P < 0.05$ and, * ⇔ $P < 0.01$, * * ⇔ $P < 0.001$, * ** ⇔ $P < 0.0001$

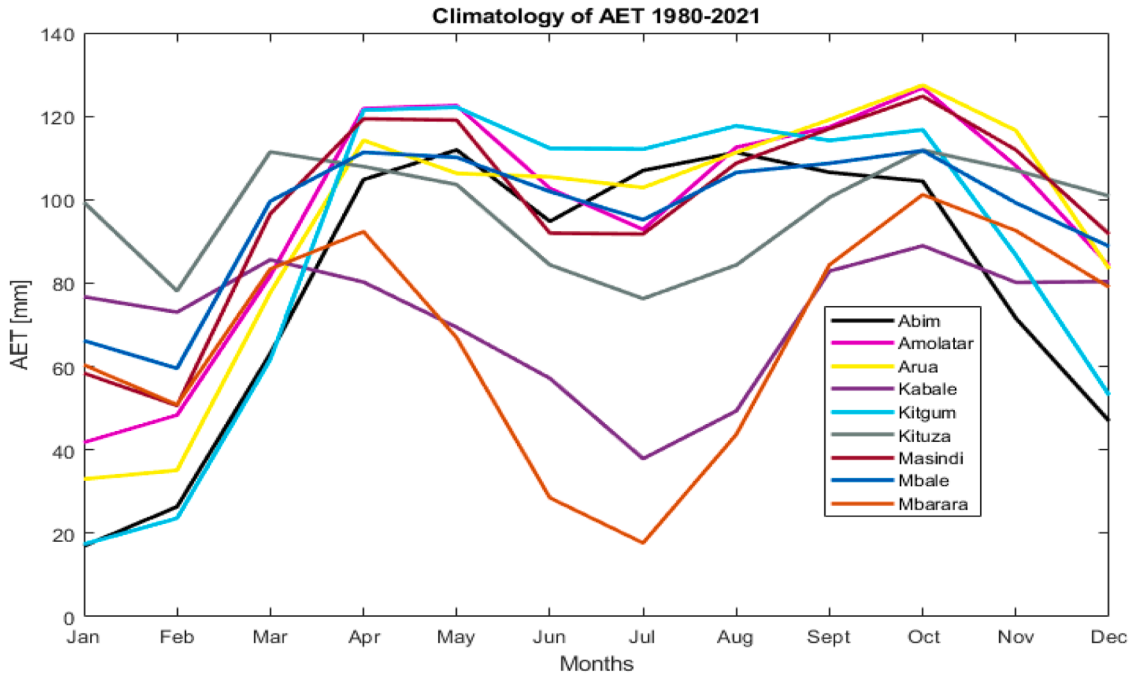

Fig. 4. Annual Cycle of Actual Evapotranspiration in the RCGR.

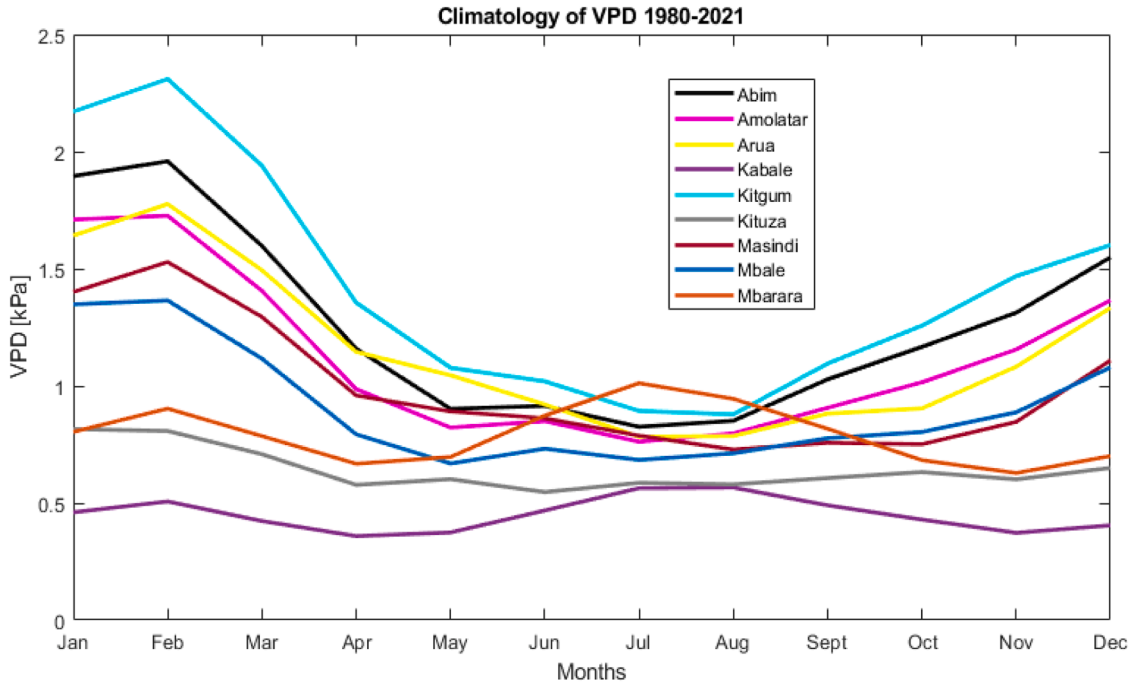

Fig. 5. Annual cycle of the Vapor pressure deficit in the RCGR.

Notably, about two of the three stations, for the first five months the calendar year, FAPAR of Amolatar can be regressed perfectly from Masindi FAPAR and vice versa. Alternatively, other stations assume distinct patterns, for example, Abim's annual FAPAR cycle has a dome-shaped pattern that roofs in the months of June-August at 0.65 then deteriorates up to 0.25 in December and January when it starts rising again. The other two stations of Mbale and Kituza also exhibit distinct annual cycles with Kituza having the least interannual variability with the station recording 0.50 and above throughout the year. FAPAR in the two other stations of Mbale and Mbarara can also be classified as less interannually variable.

Note that the extracted geo-points for this study for Kitgum and Arua had missing data for FAPAR therefore the stations were omitted in the analysis.

4.2. *Long-term trends in monthly essential climate variables*

MKSSE results revealed increasing and decreasing trends in monthly mean VPD in RCGR except at Kitgum and Abim stations. That's, significantly increasing trends in Amolatar, Kabale, Mbale and Mbarara, and, significantly decreasing trends in Arua, Kituza and Masindi stations. As such, H_o was rejected for Arua with a $P < 0.001$, Kituza with a

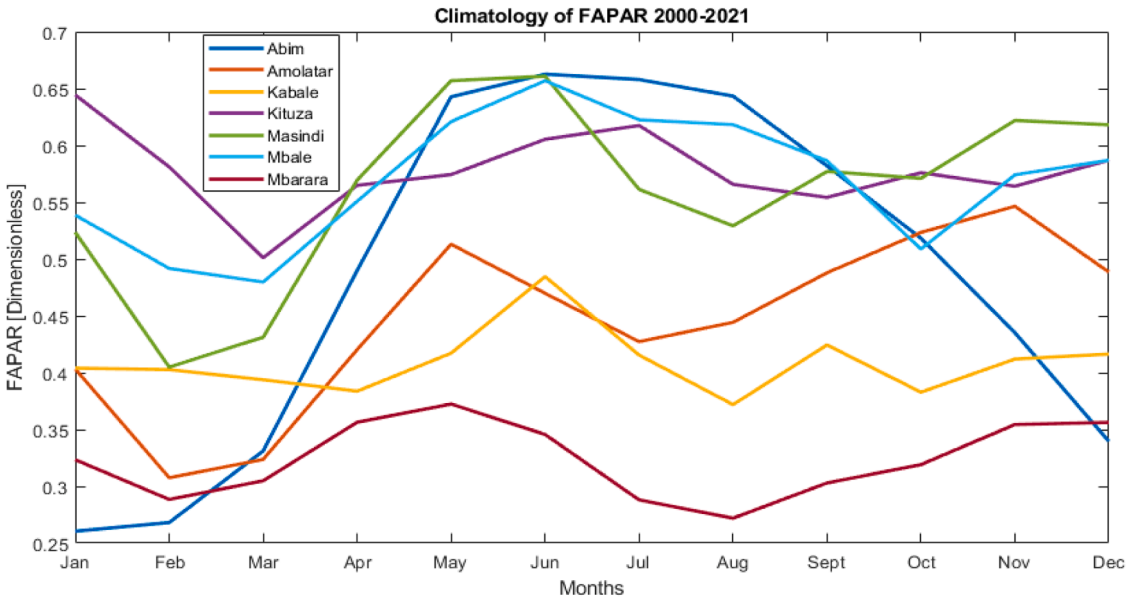

Fig. 6. Annual cycle of FAPAR in the RCGR.

$P < 0.05$, Masindi with a $P < 0.05$ for decreasing trends and Amolatar with a $P < 0.001$, Kabale with a $P < 0.0001$, Mbale with a $P < 0.01$ for increasing trends with slopes of −0.0006, −0.00001, −0.0002 and 0.0004, 0.0002, 0.0002 respectively but maintained for the remaining two stations (Kitgum and Abim). Furthermore, Amolatar is seen to have an evaporative demand increasing twice the rate of Kabale and Mbale.

While as, decreasing trends in 8-daily FAPAR are observed in Kabale, Kituza, Mbale and Mbarara stations for the period (2000–2021). Therefore, H_o was rejected for Kituza with a $P < 0.01$, Kabale with a $P < 0.05$, Mbarara with a $P < 0.0001$ and Mbale with a $P < 0.01$ for decreasing trends with slopes of −0.0006, −0.0003, −0.002 and −0.0003 respectively and maintained for Amolatar, Abim and Masindi where the trends where not significant at $P < 0.05$.

There are no observed long-term trends in CWB and AET over the study region except Arua where AET was decreasing at 0.05 level of significance.

4.3. Dynamics of the climate water balance in RCGR

Spiral plots were used to visualize the dynamics of CWB over the selected stations in the RCGR (Fig. 7). As described in the previous subsection, the annual cycle of CWB in the RCGR is highly variable owing to seasonal variation in both AET and Precipitation over Uganda. The general range is between −100 mm (deficit) and 600 mm (surplus). From Fig. (7), the periods of water surplus and deficits for the selected hybrid stations in RCGR for the period (1980–2021) are depicted.

Table 5 below shows a summary of water deficit and surplus classification for the selected stations in the RCGR of Uganda. Kituza and Kabale stations are the only stations free from water deficits, while as Mbarara experienced the longest period of deficit (4 months). The longest water surplus period is observed in Kabale for a period of up to 9 months.

4.3.1. BEAST for AET and VPD in RCGR

Meteorological and hydrological timeseries globally are known for their inherent non-linearity. In order to understand their dynamics in detail therefore, it was prudent to diagnose the timeseries further for points of change, seasonal changes and short lives trends details. Note however, only selected AET and VPD results for selected stations have been included in this study for the interest of space. As seen from Fig. (8), the decreasing trend in AET over Arua detected by MKSSE is confirmed by BEAST along with its start time (1990), followed by points of abrupt changes in 2005 and 2012 and, a pause since early 2012. Although there were no long-term trends in monthly AET over Kituza and Mbale, BEAST could still reveal the stochasticity of AET trends over Kituza (Fig. 9) in the mid 1980's, early 2000's, 2015 and recently in 2020 associated with trend anomalies since 1982 with periodicities of 1–4–15–2–11–4 years corresponding to years 1982–1983: 1983–1987: 1987–2002: 2002–2004: 2004–2015: 2015–2019 respectively with occurrence probabilities well above 0.1 since 2004. Furthermore, the inter-seasonal and inter-decadal perturbations in even the considerably stable AET timeseries were revealed. For example, the 20-year sequential (decreasing and increasing) trend in Mbale AET (Fig. 10) between 1995 and 2015 was associated with changing seasonality with very low occurrence probabilities.

For VPD, Figs. (11–13), the long-term trend in Amolatar VPD (Fig. 11) was confirmed and interannual and inter-seasonal recent abrupt changes were revealed. The increasing trend in long-term monthly Kabale VPD (Fig. 12) characterized with abrupt changes since 2002 was also confirmed, and, recent abrupt changes in Kituza monthly VPD (Fig. 13).

VPD decompositions for Amolatar for example revealed abrupt changes in trends starting in 2009 with periodicities of 5–3–1–2–1 years between sparking seasonality fluctuations since late 2015. While as VPD in Kabale was associated with abrupt changes since 2001 with periodicities of 3–4–0.65–4–0.8–4–2–0.4–1 years between. Trend instabilities were also observed at Kituza at the end of 1991 to mid-1992, 2001, 2004–2005, 2006–2007, 2016–2017, 2018 and 2019 with a probability of occurrence above 0.05.

4.3.2. Spatiotemporal trends in annual potential evapotranspiration and net primary productivity

In order to understand the spatiotemporal trends in annual PET and NPP between (2001–2021), spatio-MKSSE was adopted. For spatiotemporal trends, the PET data at an annual resolution for the period (2001–2021) was considered since its companion yield proxy (NPP) data was only available at an annual temporal resolution and a spatial resolution of 500 m for both datasets for that period. First, spatial interpolation was used in mapping the magnitude of time averaged Annual PET and NPP data Fig. (14).

The diversity of both annual PET and NPP in RCGR was clearly revealed including that of the regions outside the RCGR. For PET

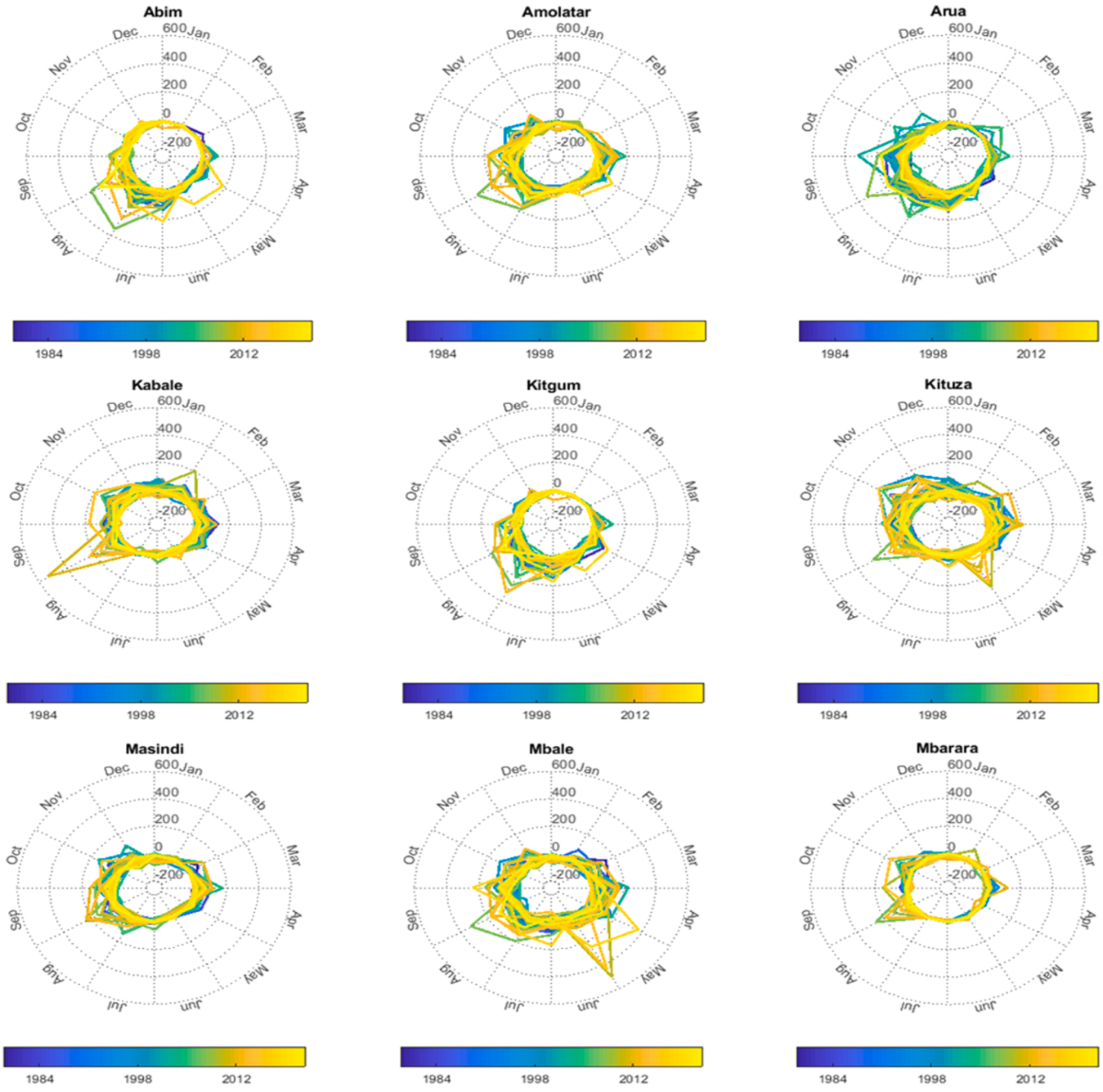

Fig. 7. Monthly CWB at selected stations in the RCGR for the period 1980–2021.

Table 5
Classification of the annual cycle of CWB in selected stations in RCGR.

Hybrid Stations									
CWB Mode	**Abim**	**Amolatar**	**Arua**	**Kabale**	**Kitgum**	**Kituza**	**Masindi**	**Mbale**	**Mbarara**
Deficit	Dec-Feb	Dec	Nov-Jan	_____	Dec-Feb	_____	Dec-Jan	Dec	Dec, May-July
Balance	Mar-May, Oct-Nov	Nov, Jan-Feb, May-Jun	Feb-May, Oct	May-Jul	Oct-Nov, Mar-Apr	Dec-Jan, Jun-Jul	Oct-Nov, Mar-Apr	Nov, Jan-Feb	Nov, Jan-Feb
Surplus	Jun-Sept	Jul-Oct	Jun-Sept	Aug-Apr	May-Sept	Feb-May, Aug-Nov	May-Sept	Mar-Oct	Mar-Apr, Aug-Oct

(Figs. 14a), up to 5 major homogenous classes and 10 sub-classes with an average buffer magnitude of major class and sub-class being 200mmyr^{-1} and 100mmyr^{-1} respectively. The highest annual PET was observed in the North Eastern part of the RCGR and country in general while the lowest in the South western part with totals that can go as high as $>$ 3000mmyr^{-1}and as low as $<$ 1200 mmyr^{-1} respectively. Mean

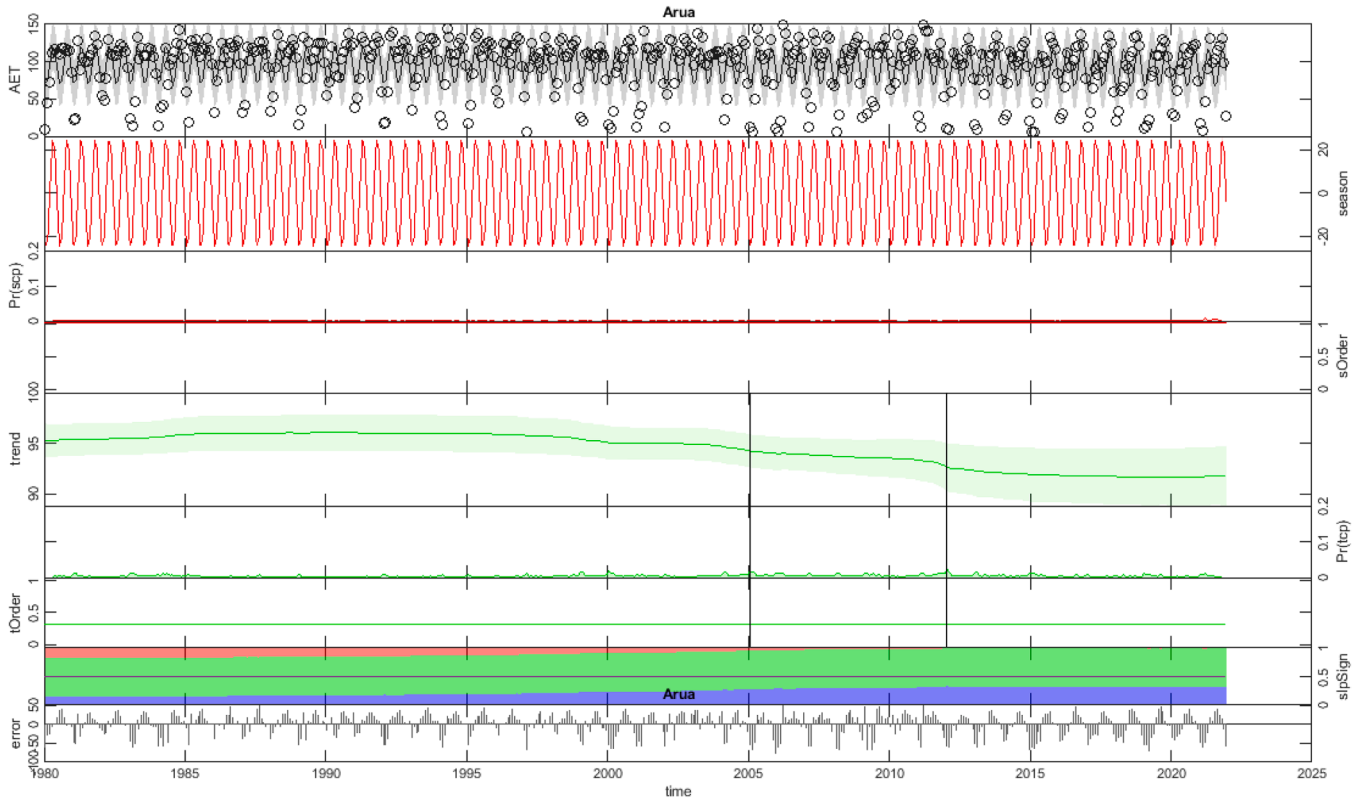

Fig. 8. Decomposition of Arua Actual Evapotranspiration into Season and sequential trends.

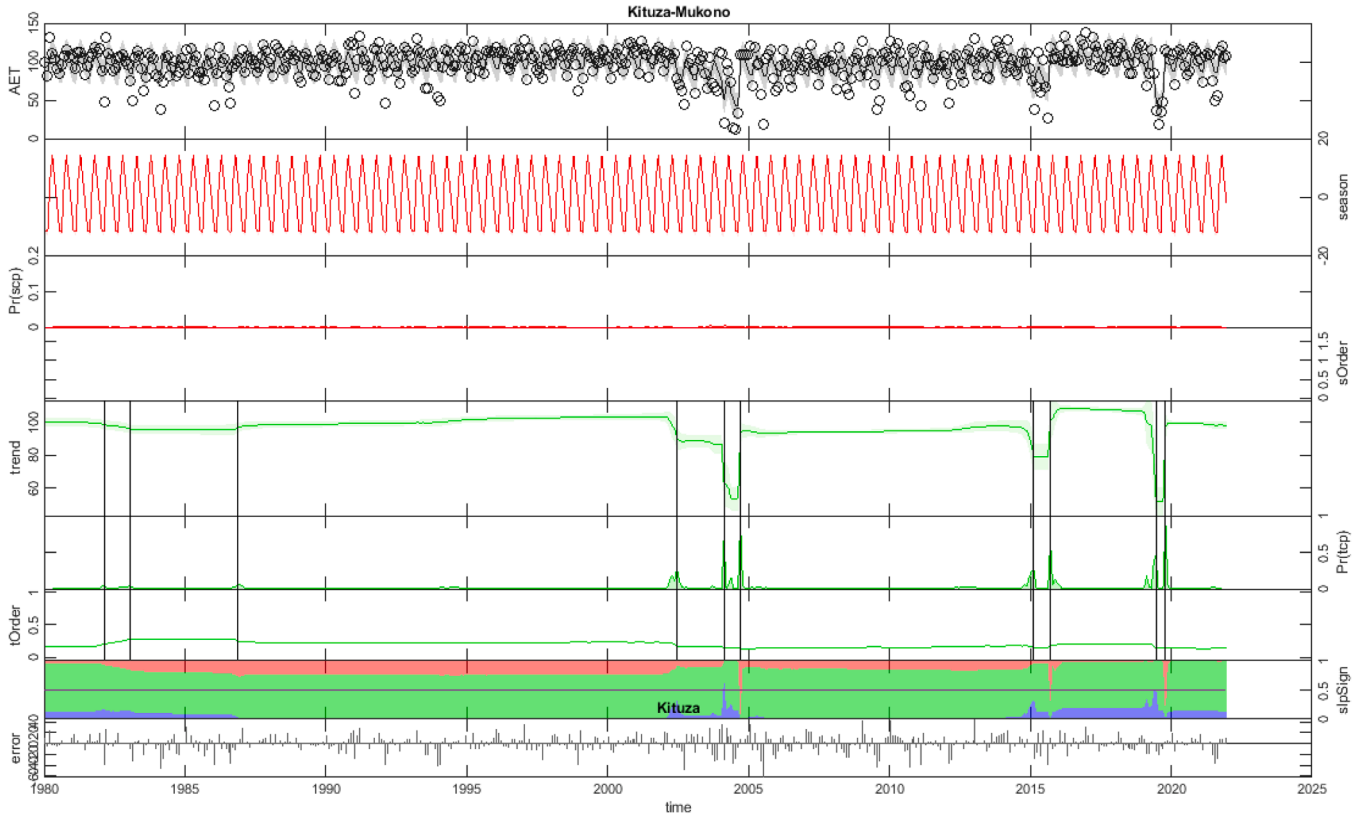

Fig. 9. Decomposition of Kituza Actual Evapotranspiration into Season and sequential trends.

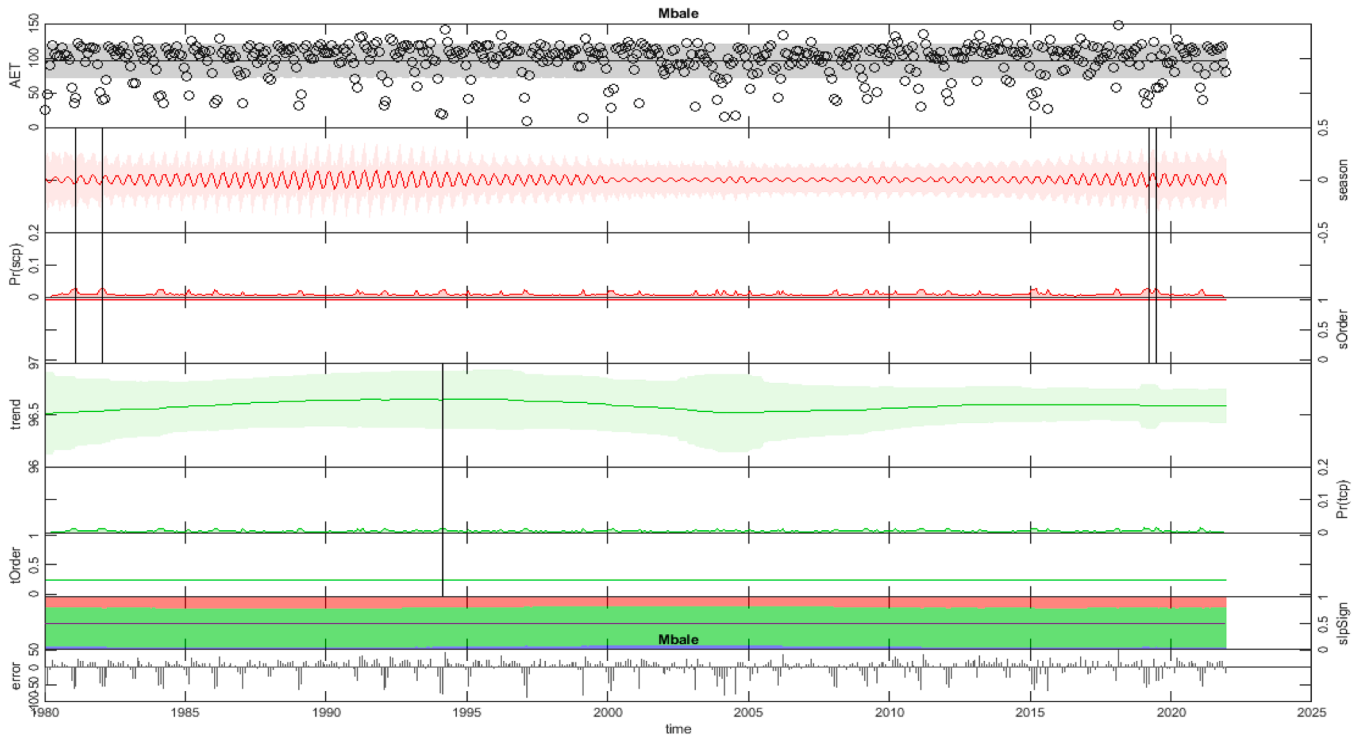

Fig. 10. Decomposition of Mbale Actual Evapotranspiration into Seasons and sequential trends.

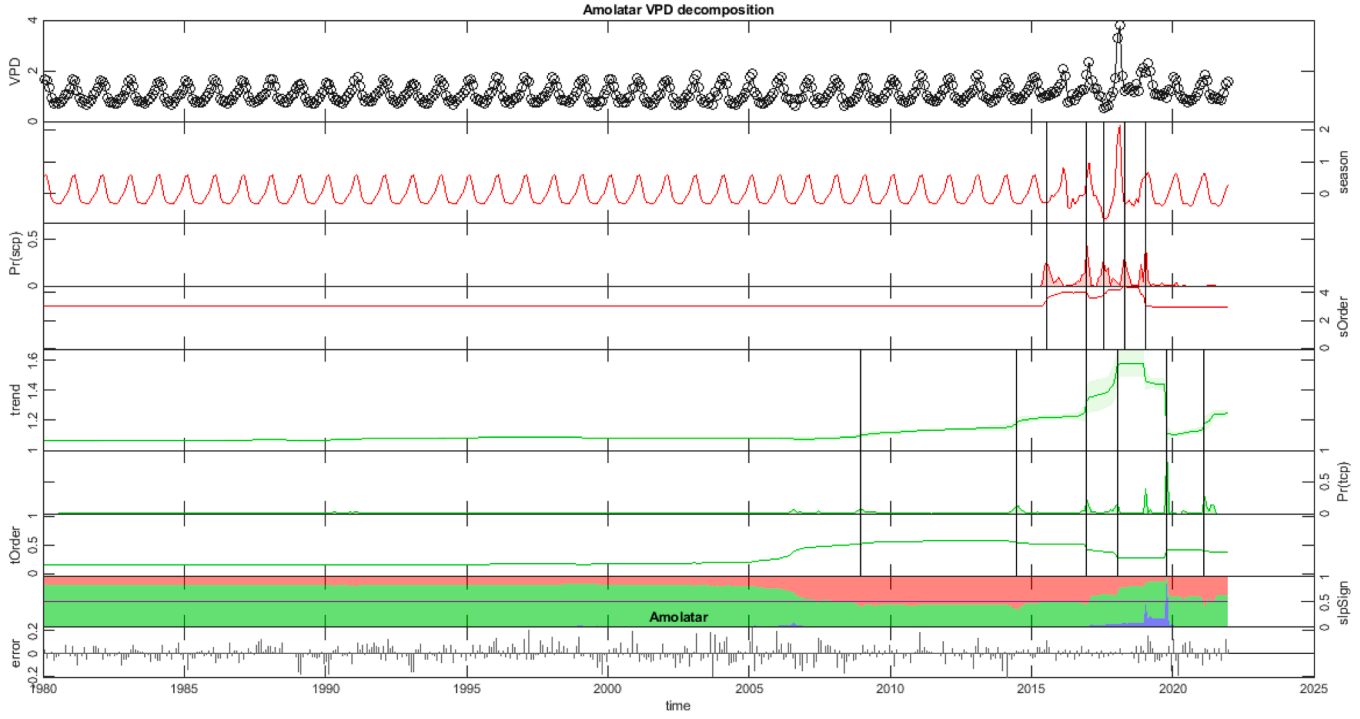

Fig. 11. Decomposition of Amolatar Vapor pressure deficit into Season and sequential trends.

annual PET generally assumes a diagonal SW-NE spatial trend. On the other hand, Mean Annual NPP (Fig. 14b) was observed to be inter-heterogenous with no clear distinction based on latitude. However, the Central-western part of the RCGR was generally more productive than the adjacent areas. The productivity in the RCGR can go as high as 2 $KgCm^{-2}yr^{-1}$and as low as zero.

As for trends, (Fig. 15), decreasing and increasing spatiotemporal trends in both Annual PET and NPP were observed in the RCGR. For PET (Fig. 15a), a general decreasing trend was detected in over 70 % of the RCGR of Uganda at an average rate of −8 $mmyr^{-1}$ for the period (2001–2021). On the other hand, NPP (Fig. 15b) was found to be increasing significantly in over 60 % of the RCGR at an average of $30gCm^{-2}yr^{-1}$ and as well decreasing significantly at an average of $-20gCm^{-2}yr^{-1}$ in about 5 % of the RCGR.

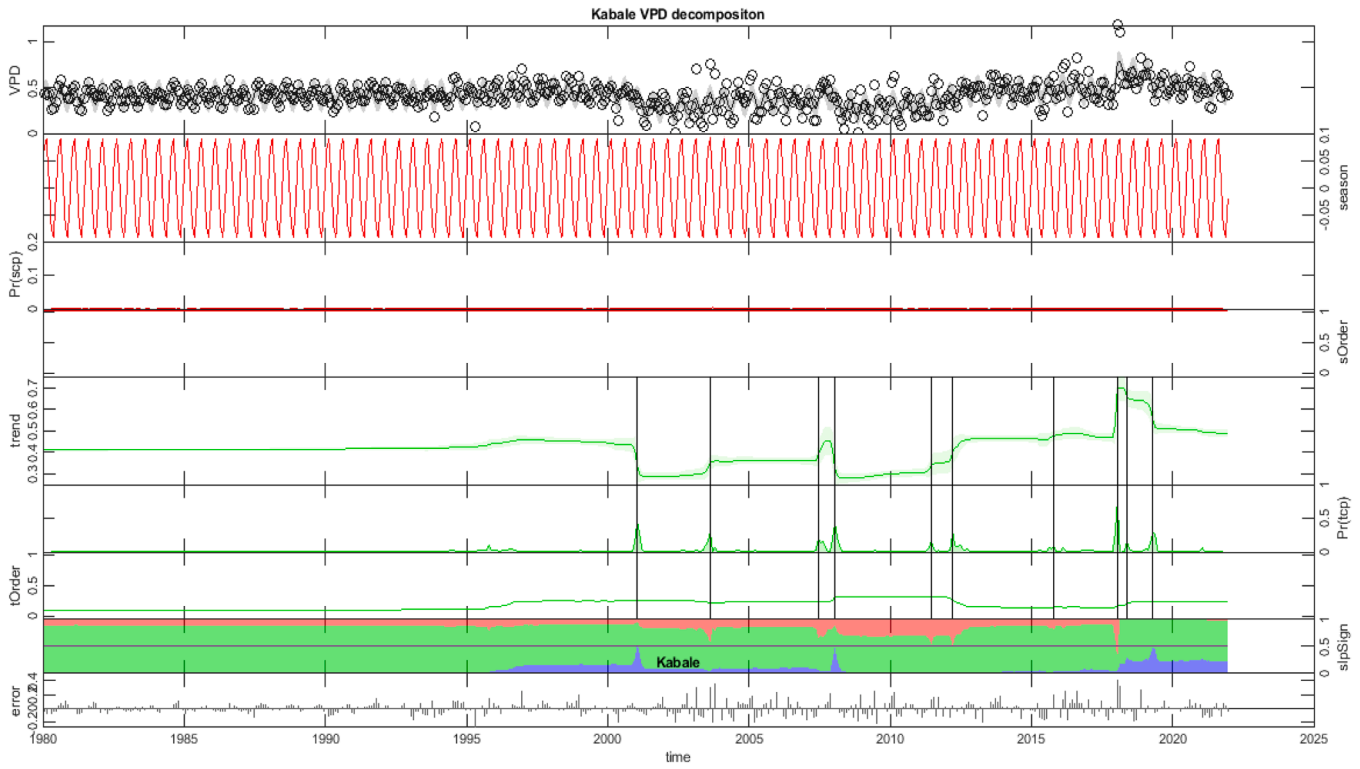

Fig. 12. Decomposition of Kabale Vapor pressure deficit into Season and sequential trends.

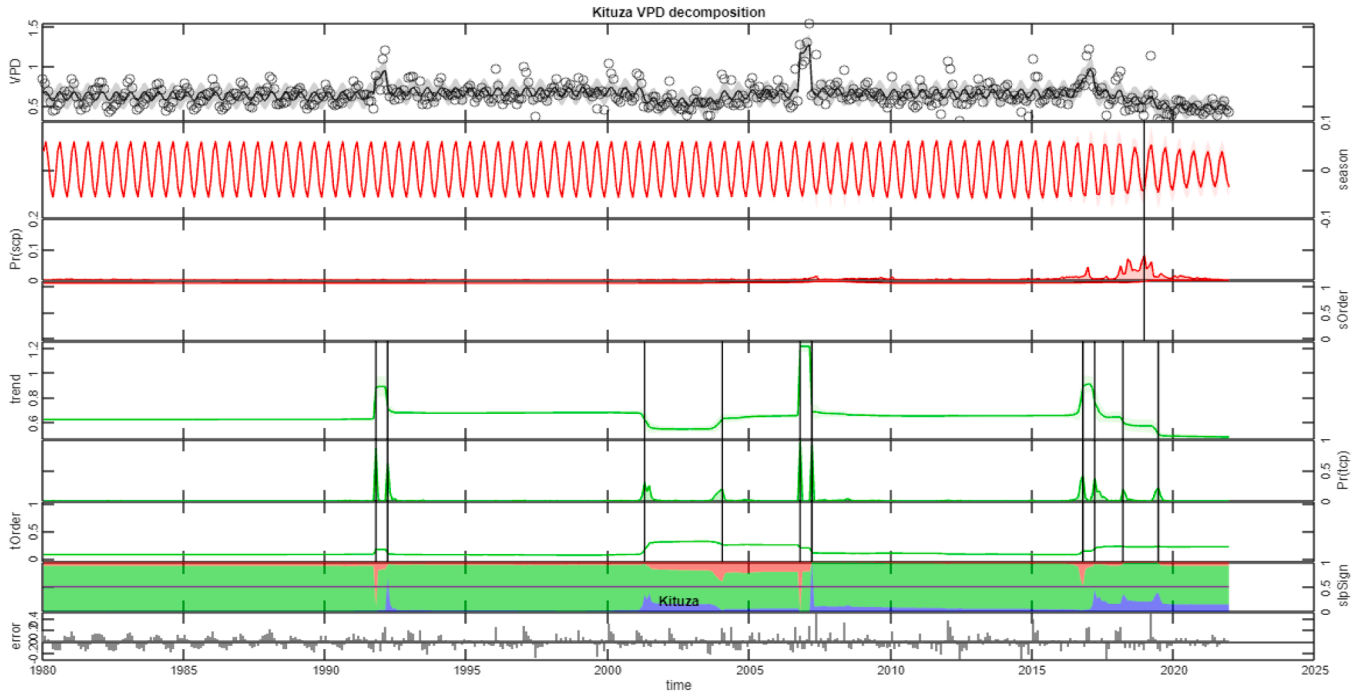

Fig. 13. Decomposition of Kituza Vapor pressure deficit into Season and sequential trends.

4.3.3. EOFs for PET

In order to demystify the underlying drivers of PET a major determinant of productivity in RCGR, we employed EOF analysis. And, from the EOF analysis, we considered the leading 4 modes that together account for 97 % explained variance in annual PET along with their amplitudes (PCs) expressed as correlations for the period 1980–2021.

Results summarized in Figs. 16 and 17 for EOF modes and PCs respectively show that highest variance (84.3 % explained variance) of annual PET in the RCGR and beyond corresponds to the dominant first EOF mode and can be explained by the leading PC1. This is followed by 9.1 %, 2.5 % and 1.3 % covariance for the 2^{nd,} 3rd and 4th EOF modes respectively. The timeseries of the four leading PCs reveal episodes of high modulations in PET over time especially during 4th and 3rd decades of the study period (1980–2021) for PC2 and PC4 respectively.

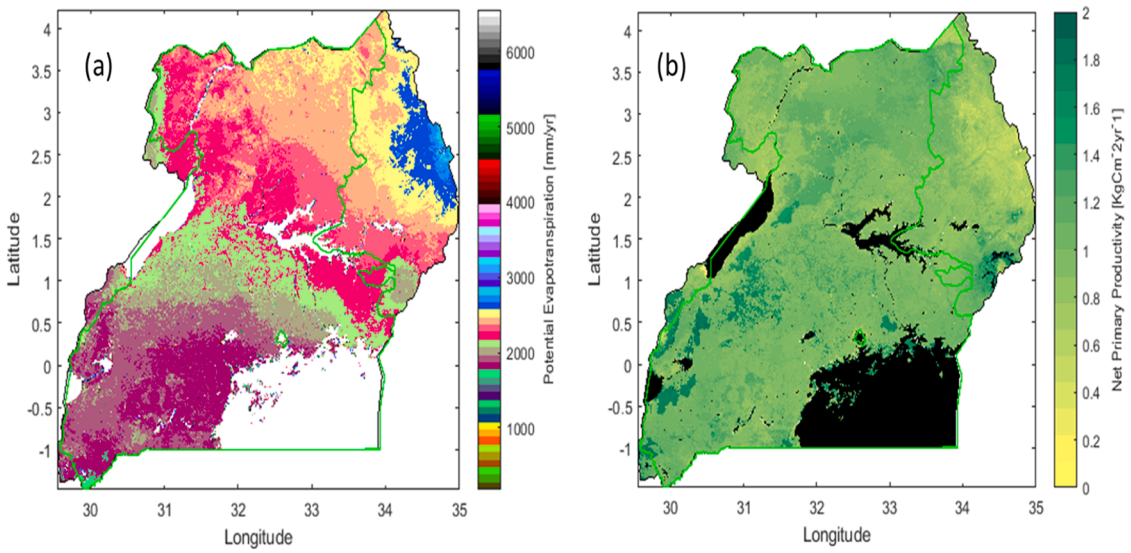

Fig. 14. Mean Annual PET(a) and NPP(b) for the period 2001–2021. The RCGR is shown by the lime-green boundary.

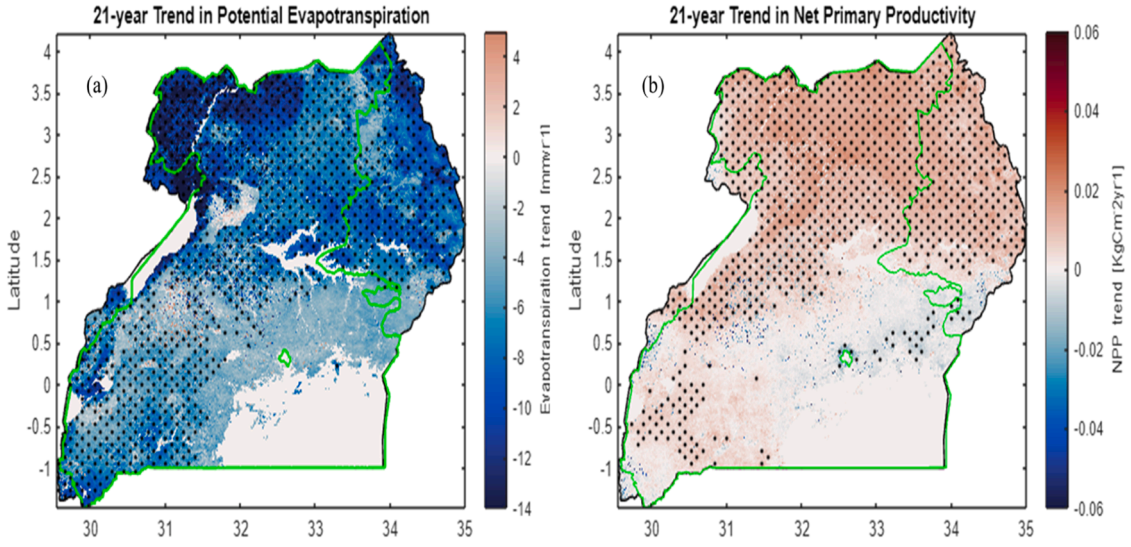

Fig. 15. Trends in Annual PET(a) and NPP(b) for the period 2001–2021. Stipples indicate areas where the trend was significant at 0.05 level of significance.

The physical mode responsible for the first EOF is the same for most parts of the RCGR except Arua, Kasese, Kabale and Mbale. However, the highest variance of PET is mainly constrained in the North Eastern stretch of the RCGR and beyond. The second EOF mode able to explain 9.1 % variance in PET shows two distinct covariances. That's, the Northern negative cluster stretching meridionally from Lake Kyoga spanning Amolatar, Abim, and Kitgum stations and the Southern positive cluster spanning Kituza, Mbarara, Masindi and Kabale stations. The 3rd EOF mode that accounts for 2.5 % of the PET variance reveals significant positive and negative covariances of PET with a slant longitudinal separation confining the negative covariance in the Albertine-graben region and positive covariance East of the Albertine-graben region. However, the 4th EOF mode that accounts for 1.3 % of the variance revealed a strong negative covariance over Wes Nile (Arua), Lake Kyoga Basin (Amolatar), Acholi region (Kitgum) and Central (Mukono) and, positive covariance over the South Western Stretch (Kabale)

4.3.4. Association between PET and NPP in the RCGR

Fig. 17: A strong negative correlation was revealed in the Northern and parts of the Southern stretch of the RCGR. While as strong and mild positive correlations were observed in Central (Kituza), Elgon region (Mbale) and Central Western (Kasese, Hoima) parts of the RCGR of the RCGR. PET is able to explain $>$ 80 % of the variation in NPP of the greater Northern part of the RCGR and beyond. That's, an increase in PET by 1 unit in areas of Arua, Kitgum, Masindi, Abim, Amolatar and some South and South western parts results into 0.8 units reduction in productivity and vice versa. Conversely, over Central (Kituza, Buikwe, Jinja), Western (Kasese) and South Western (Kabale) RCGR, an increase in PET by 1 unit was associated with 0.8, 0.6 and 0.5 uint inncreases productivity respectively.

5. Discussions

5.1. Climatology of selected agrometeorological variables

The observed uniformity in the annual cycle AET in the stations within the Lake Victoria basin can be attributed to precipitation homogeneity (Basalirwa, 1995) within these regions since this is the primary water input. While as the higher AET in western highlands, Lake Kyoga and Lake Victoria basin stations can be explained by the balance

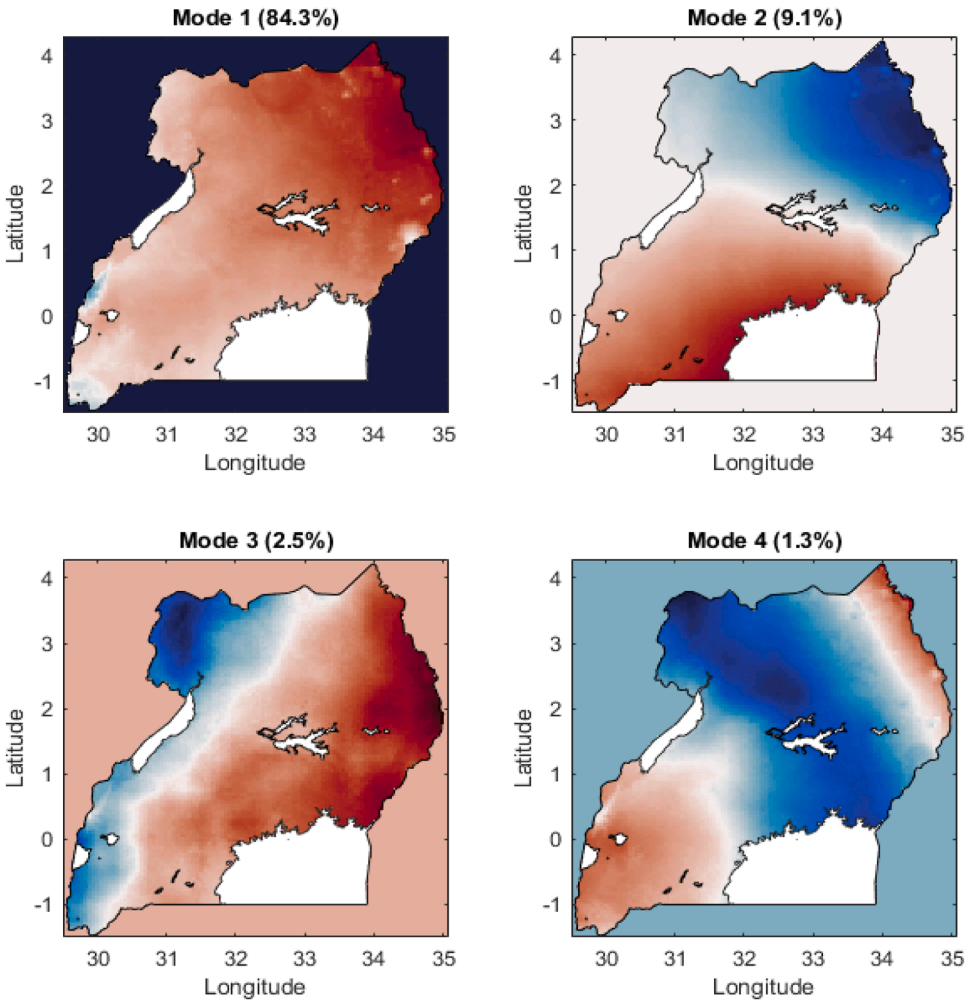

Fig. 16. The first four Annual PET EOF modes and their corresponding explained variances.

between the available water in form of soil moisture following the bimodal rainfall season characterized by the two Inter-Tropical Convergence Zonations (ITCZs) (Basalirwa, 1995; Funk et al., (2012) and the high irradiance associated with elevated atmospheric evaporative demand to drive the evapotranspiration process compared to the Northern and North eastern regions. The results are largely in agreement with a recent study by Wamucii et al. (2021) over East Africa although their study considered simulated actual Evapotranspiration.

On the other hand, the elevated VPD in Northen part of the RCGR compared to the Southern regions can be explained by relatively higher air temperatures and lower humidity in the North. Generally, the optimal VPD threshold for plant growth is 0.8–1.2kPa with specific growth stage variations. However, studies have shown that values above 1kPa are potentially stressful for crops (Shamshiri et al., 2018; Amitrano, et al., 2021). For coffee specifically, Kath et al., (2022) showed that during fruit development yield declines rapidly above 0.82 kPa. As such, except for 3 stations (Kituza, Mbarara and Kabale) in the Lake Victoria basin, the RCGR experiences elevated evaporative stress from December to April with major variations in magnitude per station that may significantly affect coffee yields in these regions. Conversely, the lower monthly values below 0.5kPa are associated with lower daily scale values which increase the Leaf Wetness duration a major precursor of fungal diseases such as coffee leaf rust (Bebber et al., 2016) and, increased moisture in the canopies facilitating growth of ambrosia fungus a major source of food to larvae and adult ambrosia beetles (Batra, 1963) such as the Black Coffee Twig Borer (Egonyu et al., 2014) a leading constraint in Uganda's Robusta coffee production (Kagezi et al., 2020). Consequently, Kabale areas and Kituza, Mbale (during certain periods) have favorable conditions for fungal pathogen growth and sporulation.

While as, the observed moderate to high photosynthetic activity over the remaining Central and Elgon regions can be attributed to reliable rainfall (Funk et al., 2012), favorable temperatures (Nsubuga et al., 2014; Majaliwa et al., 2015) and dominance of the croplands and forests land cover types since these cover types have a higher carbon storage capacity and rate compared to wood and grasslands. Conversely, the low FAPAR in south western stations can be attributed to high levels of cloudiness year-round which block incoming Photosynthetically active radiation limiting photosynthetic activity. FAPAR being an ECV with capabilities to pin-point crop health and growth anomalies owing to environmental stresses such as drought (Gobron et al., 2005) and biotic stresses, along with its strong linear relationship with the Normalized Difference Vegetation Index (Myneni and Williams, 1994), periods and areas such as February for Abim and February and August for Kabale with FAPAR below 0.3 can be classified as stressful periods for crop growth.

From a climate water balance view point, stations like Kituza and Kabale in Central and South western RCGR respectively are characterized with water adequate annual cycles compared to other stations. However, periods of water balance especially December in Kituza that correspond to the flowering stage of Robusta coffee in the central RCGR (Sseremba et al., 2023) may still require irrigation due to the elevated demand in water by the Robusta crop during this stage. On the other hand, excessive moisture during the months of March and April Kabale

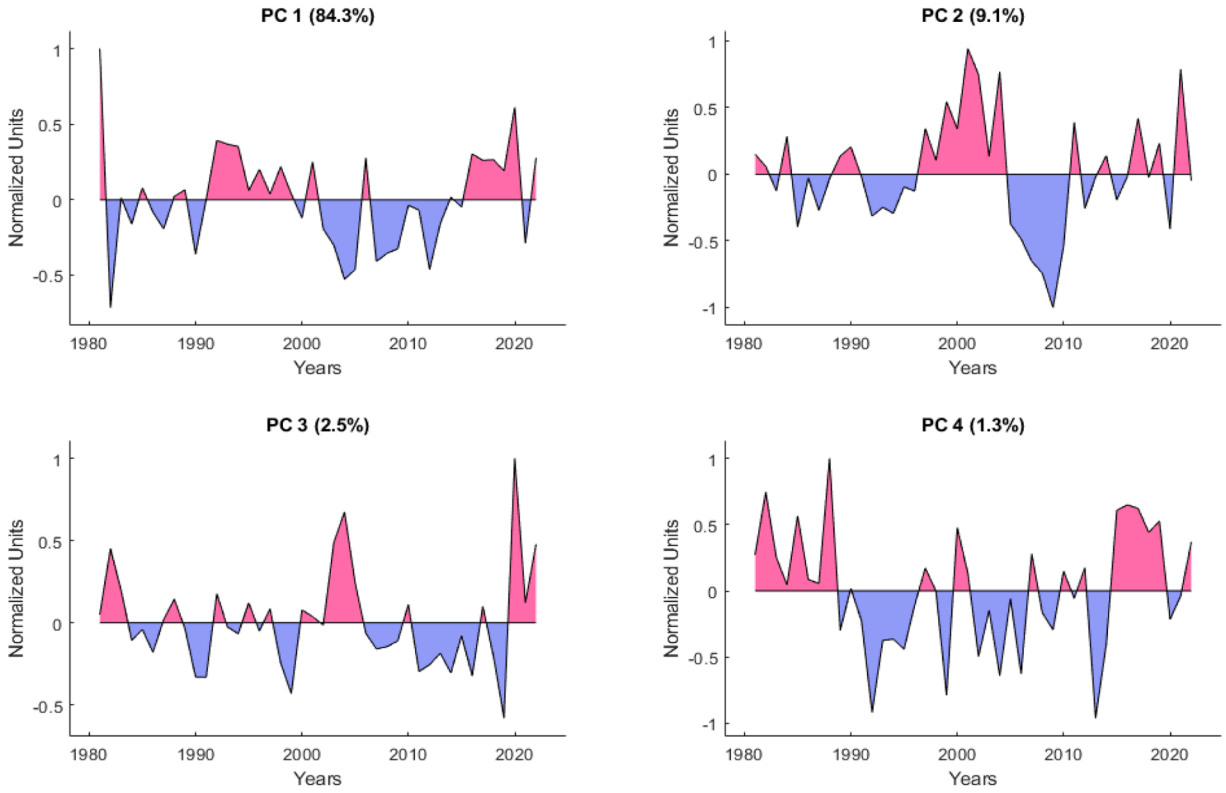

Fig. 17. Timeseries of four leading PCs.

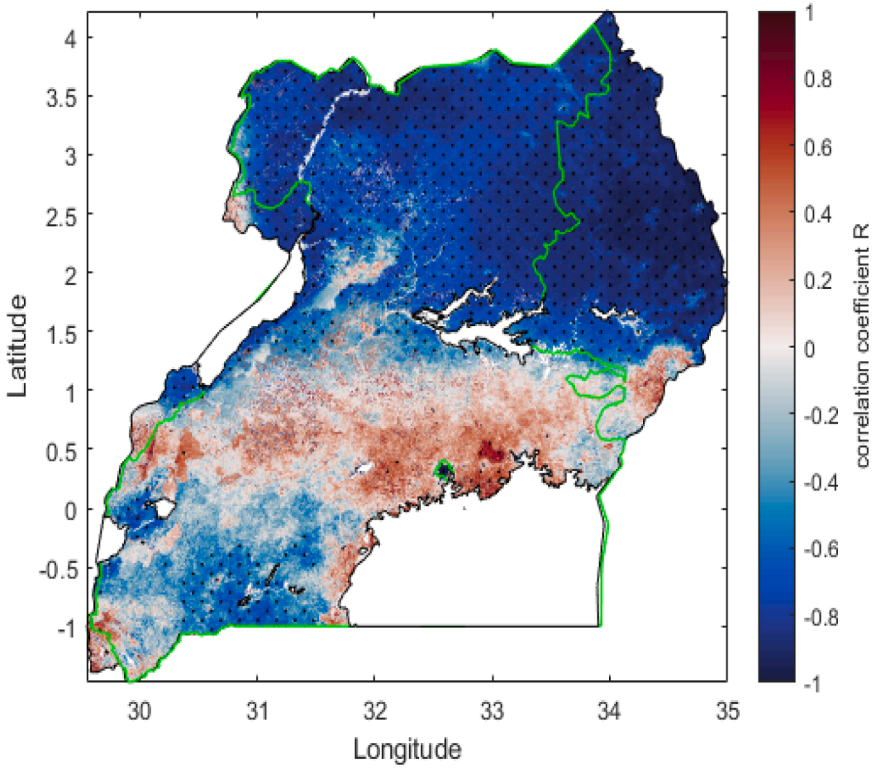

Fig. 18. Pearson' s correlation coefficients between PET and NPP in the RCGR and beyond.

and Kituza respectively may for results in the imbalance of growth regulators and promoters leading to increased vegetative growth at the expense of reproduction drastically reducing the number of flowers (Titus and Pereira, 2017). Although coffee requires a transient period of water stress to initiate it's reproductive phase (Carr, 2001), stations like Mbarara, Kitgum and Abim associated with longer periods of water

deficit during months of Robusta coffee reproduction require extra water in form of irrigation to abate coffee yield loses both terms of quality and quantity (Tran et al., 2021; Waqas et al., 2024).

5.2. Temporal and Spatiotemporal dynamics of selected Agrometeorological variables in RCGR

5.2.1. Long-term Monotonic trends in VPD and FAPAR in RCGR

The observed decrease in AET over Arua may signals reductions in evaporative demand which can be evidenced by the observed decreasing trends in VPD. Similarly, these results are in agreement with Wamucii et al. (2021) on terms of trend direction.

On the other hand, reduction in VPD can be explained by increasing humidity suppressing the evaporative demand while as, increases in VPD can be attributed to increasing temperatures as a result of global warming. Notably, both the reduction and gains in VPD pose serious risks to Robusta coffee pest and disease management (Bebber et al., 2016) and water use efficiency and management (Grossiord et al., 2020) in the RCGR consequently affecting yields. For example, coffee yields are expected to decline in Mbarara and Mbale where the VPD during fruit development is already above the 0.82 kPa threshold (Kath et al., 2022) and yet continues to increase.

Likewise, the observed reduction in FAPAR with time may signal both plant or vegetation failure to photosynthesize owing to environmental stresses such as drought, an increase in atmospheric albedo due to increasing cloud cover reflecting irradiance within PAR (0.4–0.7 μm) range or changing landcover due to human activities. PAR is a major factor in assimilation of important nutrients in coffee such as Nitrogen (Luiza et al., 2006), the reduction in its absorption and or availability to coffee plants in these regions pauses direct risks on Robusta coffee yield quantity and quality.

5.2.2. Abrupt changes in seasons and trends of AET and VPD for selected stations in the RCGR

Internally, the observe instability in trends and seasons of ECVs such as AET and VPD in the RCGR can be explained by the corresponding and underlying abrupt changes in Air temperature, humidity, precipitation, land use land cover, cloud cover among others.

Externally, the abrupt changes could partly be attributed to ENSO events. For example, the 1991/92 abrupt change in trend of AET in Kituza and VPD trend fluctuation episodes of 2008 and 2011 for Kabale can be attributed to El-Nino/Southern Oscillations (ENSO) (Phillips and Mcintyre, 2000) of the El-Nino and La-Nina type respectively.

However, a considerable number of break points, seasonal fluctuations and return periods could not be convincingly explained by short-term inter-seasonal phenomena such as ENSOs, Maddening Julian oscillations or Indian ocean dipole phases but rather multiyear climate disturbances. As such, further studies on the role of long-lived atmosphere-oceanic teleconnections such as Quasi-Biennial Oscillation and Atlantic Multidecadal Oscillation (Cardil et al., 2023) in the observed trend and seasonal fluctuations.

These short lived and abrupt changes in ECVs especially VPD and FAPAR intensify the already complex Robusta coffee management challenge and can be associate with pest and disease outbreaks resulting in both resource and yield losses during the growing season.(Nilsson et al., 2020).

5.2.3. Spatiotemporal dynamics of PET and NPP

The trend magnitude range of PET in the RCGR and beyond for the period 2001–2021 is (-14−5) $mmyr^{-1}$of which the significant trend range is (-14-) *($P < 0.05$)*. As earlier observed, although our period of study is 14years lesser than that of a recent study by Onyutha et al. (2021) which considered a study period of 1979–2013 with a slight overlap into the future for the present study, still the results on PET trends are far different. For example, the mentioned study's trend magnitude range was (-18.49–11.83) $mmyr^{-1}$. The variation in the trend magnitude can be attributed to the inherent weaknesses highlighted earlier. However, there were some points of agreement on the basis of trend direction in some sections of the Northern (Arua), Western (Masindi) and some parts of south western RCGR.

PET is driven by a number of factors that include mean temperature, diurnal temperature range, relative humidity (RH), wind speeds and sunshine hours. Studies including Allen et al. (1998), Xu et al. (2006), Zhi Li et al. (2012) among others have shown that RH and number of sunshine hours are the dominant drivers of PET. Therefore, the observed decreasing trend in PET over > 70 % in the RCGR and beyond can be attributed to: (i) corresponding reductions in VPD (a proxy for RH) in Arua and Masindi regions and, (ii) corresponding reductions in FAPAR (owing to reduced number of sunshine hours/increasing atmospheric albedo (due to cloud cover)) in Kabale, Mbarara and Mbale. This is however not conclusive evidence and further studies are encouraged to assess the drivers of PET directly and independently in the RCGR. The reduction in PET nevertheless signals a system or an environment with both reducing entropy and an increasing wetness index.

The observed upward trend in NPP in the RCGR can among other factors be attributed to the reduction in evaporative stress: VPD (specifically Arua and Masindi areas), land cover change: grassland to farmland Masindi-Kyoga area (Kuule et al., 2022). About 20 % of the areas in RCGR had no significant trends ($P < 0.05$). Areas in the central, extreme west and south of the RCGR.

The reduction in productivity in Central (Kituza) and Elgon (Mbale) regions can among other factors conform to the reduction in FAPAR earlier revealed in these specific areas and, and for Mbale in particular increasing VPD, Land use land cover change: forest to farmlands (Nantumbwe and Tenywa, 2016; Kilama Luwa et al., 2021) since the former has a higher carbon storage capacity and rate (Nielsen, 2009), emergence and resurgence of new pests and diseases (Kagezi et al., 2017, 2020).

5.3. Spatial covariance and attribution of PET in the RCGR

By default, the EOFs force an orthogonal solution of the modes so as to achieve independence in at least the dominant modes of variance and as well pin point the physical drivers (Dommenget and Latif, 2002; Messié and Chavez, 2011). Although based on the corresponding PC the first EOF mode did not conform to the major external physical climate drivers such as Indian Ocean Dipole, ENSO or Madden-Julian Oscillations, the observed constrained strong positive covariance over the Karamoja region mimics the annual temperature (Majaliwa et al., 2015) and cloud cover climatology.

Similarly, the second EOF mode can be attributed to the Lake Victoria effect (Basalirwa, 1995; NICHOLSON et al., 2021) especially for the Southern positive cluster given the increase in covariance Lake Victoria-wise and vice versa. However, more research is needed to fully establish the identified pattern similarity.

On the other hand, based on it' corresponding PC, the 3rd EOF mode could be attributed to an external physical mode such as ENSOs. The spatiotemporal variations in PET in the RCGR are therefore more internal than externally driven. The need for a lengthened study on the internal drivers of PET dynamics is therefore apparent.

5.4. PET as a driver of Crop Productivity in the RCGR

The strong negative correlation between PET and NPP over most parts of the RCGR can be partly explained by the fact that PET reductions are associated with increased wetness index and reduced drought stress to crops leading to increased performance and vice versa.

On the other hand, the positive correlation in Central (Kituza), Elgon region (Mbale) and Western Central (Kasese, Hoima) parts of the RCGR shows partly that PET is not the sole driver of productivity in these regions. Firstly, either the regions are well watered with higher dryness thresholds and degrees of freedom making them barely sensitive to the

drought stress for example Kituza and Kabale with higher moisture surpluses and considerably lower VPDs. In this case increased entropy maintains system functionality than suppress. Such functionalities include nutrient uptake and assimilation (Luiza et al., 2006), water and nutrient use efficiency (Nandy et al., 2022) Or, the regions are characterized by extensive human intervention in form of irrigation, fertilizer use, good agronomic practices that offset the environmental stress.

Nevertheless, it's safe to conclude that PET can suitably tell the story of $>$ 95 % of the RCGR's productivity. Further studies are however encouraged to further explore this relationship.

6. Conclusions

In this study, a thorough assessment of agroclimatic variables in both the temporal and spatiotemporal domains over the Robusta coffee growing region (RCGR) of Uganda revealed; stability of variables such as Actual Evapotranspiration (AET) and Climate Water Balance (CWB), and instability in Vapor pressure deficit (VPD), Potential Evapotranspiration (PET), Fraction of Absorbed Photosynthetically Active Radiation and Net Primary Productivity (NPP) characterized by both decreasing and increasing trends as well as changing seasonality in both the short and long run; a low sensitivity of PET to largescale atmosphere-ocean circulations such El-Nino/Southern Oscillations as well as its strong correlation with NPP. These results specifically call for action in terms of soil water conservation and management practices intensification especially in Amolatar, Mbarara, Kitgum, Mbale where longer periods of water deficits have been observed to compensate for the increasing evaporative demand and as well ensure a balanced water-use efficiency for the Robusta coffee crop as well as farmer trainings on crop canopy managements such as shade tree management during periods or in areas where FAPAR is low to ensure coffee trees intercept the little available PAR. On this note therefore, studies are recommended to expose directly the factors behind the observed reductions in FAPAR, increasing VPD as well prolonged water deficits.

Funding

This project was funded by the United States Agency for International Development (USAID) through the Enhanced Resilience for Agricultural systems and Livelihoods project (ERAAL), grant number AG-4826.

Appendix

Quality control of TAMSATand TERRA climate data

CRediT authorship contribution statement

Anthony Gidudu: Writing – review & editing, Resources. **Geoffrey Arinaitwe:** Project administration, Funding acquisition. **Mihai Voda:** Writing – review & editing, Supervision, Resources, Funding acquisition. **Ronald MSc Ssembajwe:** Writing – original draft, Methodology, Investigation, Formal analysis, Data curation, Conceptualization. **Ronald Opio:** Writing – review & editing. **Judith Kobusinge:** Writing – review & editing, Investigation. **Frank Mugagga:** Writing – review & editing. **Yazidi Bamutaze:** Writing – review & editing, Resources. **Catherine Mulinde:** Writing – review & editing, Supervision, Conceptualization. **Saul D. Ddumba:** Writing – review & editing, Supervision, Methodology, Conceptualization. **Godfrey H. Kagezi:** Writing – review & editing, Supervision, Resources, Project administration, Funding acquisition, Conceptualization.

Declaration of Competing Interest

The authors declare that they have no known competing financial interests or personal relationships that could have appeared to influence the work reported in this paper.

Acknowledgments

The first author wishes to thank the support from the European Commission through the Erasmus+ student exchange program and Dimitrie Cantemir University IR-BE-73776 project which enabled the publication of this paper. We also acknowledge the financial and technical support from RCMRD-GMES Africa Project on access to and validation of satellite products used in this study.

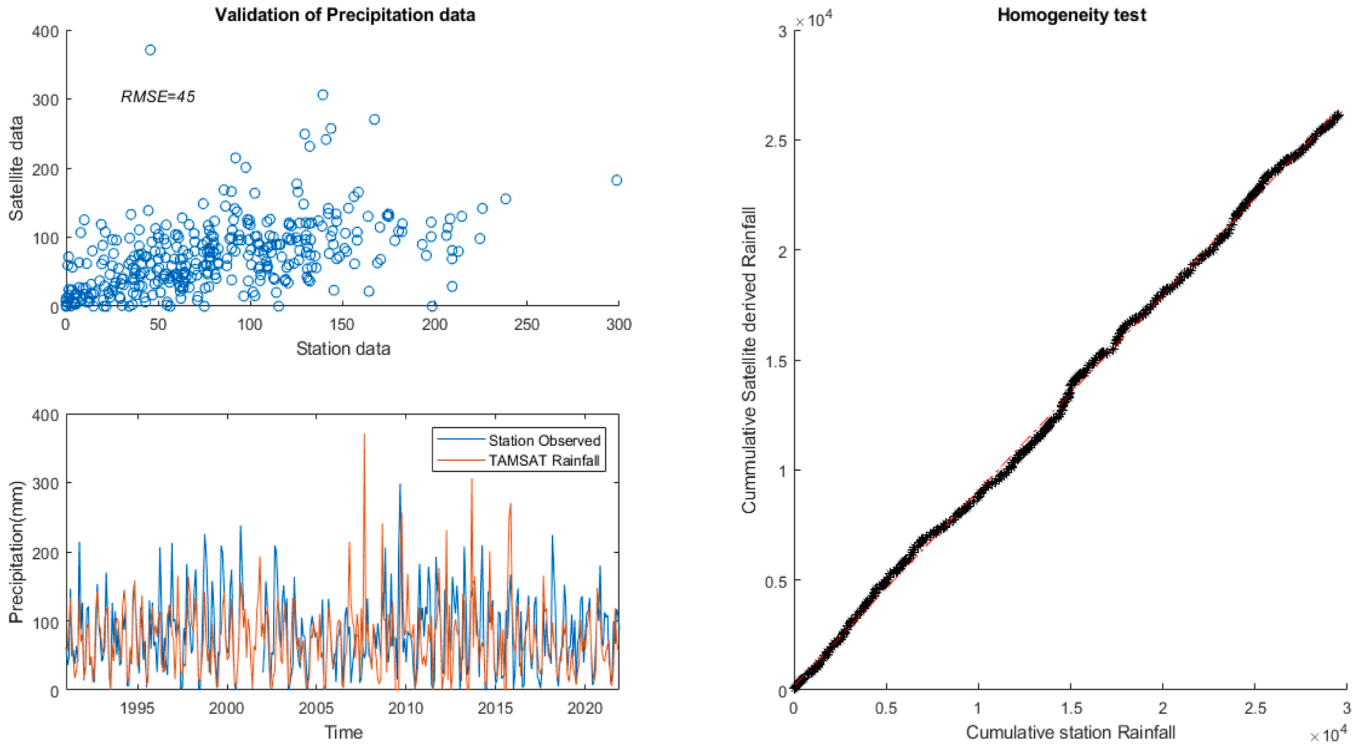

Appendix 19. Validation results of TAMSAT satellite Rainfall estimates from Mbarara

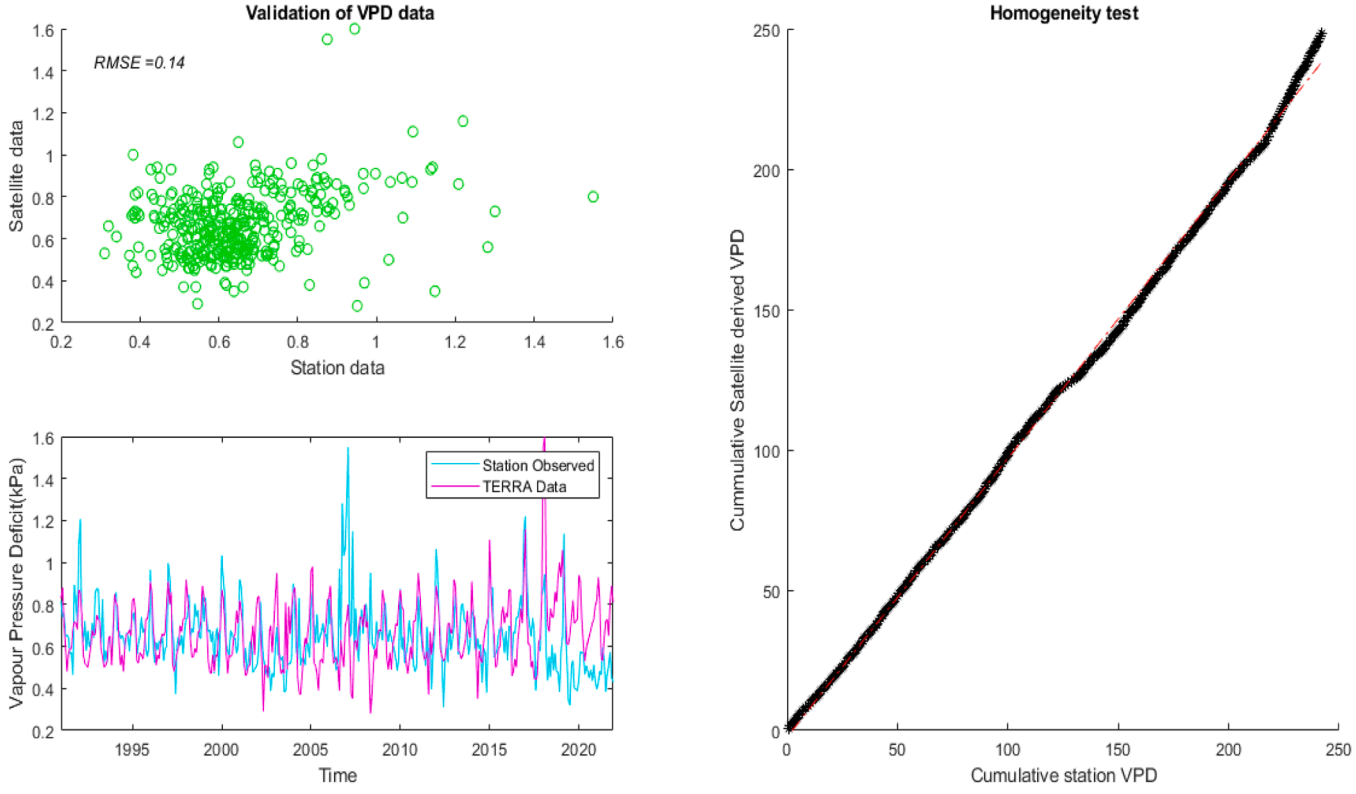

Appendix 20. Validation results of TERRA VPD estimates from Kituza (Mukono) station

Data availability

Data will be made available on request.

References

Abatzoglou, J.T., Dobrowski, S.Z., Parks, S.A., Hegewisch, K.C., 2018. TerraClimate, a high-resolution global dataset of monthly climate and climatic water balance from 1958-2015. Sci. Data 5, 1–12. https://doi.org/10.1038/sdata.2017.191.

Alashan, S., 2020. Combination of modified Mann-Kendall method and Şen innovative trend analysis. Eng. Rep. 2 (3), 1–13. https://doi.org/10.1002/eng2.12131.

Allen, R.G., Pereira, L.S., Raes, D., & Smith, M. (1998). Crop Evapotranspiration: Guidelines for computing crop water requirements-FAO Irrigation and Drainage Paper56 (1998).

Amitrano, C., Rouphael, Y., De Pascale, S., De Micco, V., 2021. Modulating vapor pressure deficit in the plant micro-environment may enhance the bioactive value of lettuce. Horticulturae 7 (2), 1–15. https://doi.org/10.3390/horticulturae7020032.

Amitrano, C., Rouphael, Y., Pannico, A., De Pascale, S., De Micco, V., 2021. Reducing the evaporative demand improves photosynthesis and water use efficiency of indoor cultivated lettuce. Agronomy 11 (7). https://doi.org/10.3390/agronomy11071396.

Anapalli, S.S., Fisher, D.K., Pinnamaneni, S.R., Reddy, K.N., 2020. Quantifying evapotranspiration and crop coefficients for cotton (Gossypium hirsutum L.) using an eddy covariance approach. Agric. Water Manag. 233 (2019), 106091. https://doi.org/10.1016/j.agwat.2020.106091.

Anderson, M.C., Zolin, C.A., Sentelhas, P.C., Hain, C.R., Semmens, K., Yilmaz, M.T., Gao, F., Otkin, J.A., Tetrault, R., 2016. The Evaporative Stress Index as an indicator of agricultural drought in Brazil: an assessment based on crop yield impacts. Remote Sens. Environ. 174, 82–99. https://doi.org/10.1016/j.rse.2015.11.034.

Asfaw, D., Black, E., Brown, M., Nicklin, K.J., Otu-larbi, F., Pinnington, E., Challinor, A., Maidment, R., Quaife, T., 2018. TAMSAT-ALERT v1 a N. Framew. Agric. Decis. Support 2353–2371.

Basalirwa, C.P.K., 1995a. Delineation of Uganda into climatological rainfall zones using the method of principal component analysis. Int. J. Climatol. 15 (10), 1161–1177. https://doi.org/10.1002/joc.3370151008.

Batra, L.R., 1963. Ecology of ambrosia fungi and their dissemination by beetles. Kans. Acad. Sci. 32 (2), 80–84. https://doi.org/10.2307/3626562.

Bautista, F., Bautista, D., Delgado-Carranza, C., 2009. Calibration of the equations of Hargreaves and Thornthwaite to estimate the potential evapotranspiration in semi-arid and subhumid tropical climates for regional applications. Atmosfera 22 (4), 331–348.

Bebber, D.P., Castillo, Á.D., Gurr, S.J., 2016. Modelling coffee leaf rust risk in Colombia with climate reanalysis data. Philos. Trans. R. Soc. B Biol. Sci. 371 (1709). https://doi.org/10.1098/rstb.2015.0458.

Berti, A., Tardivo, G., Chiaudani, A., Rech, F., Borin, M., 2014. Assessing reference evapotranspiration by the Hargreaves method in north-eastern Italy. Agric. Water Manag. 140, 20–25. https://doi.org/10.1016/j.agwat.2014.03.015.

Black, E., Greatrex, H., Young, M., Maidment, R., 2016. Incorporating satellite data into weather index insurance. R. Meteorol. Soc. 97, ES203–ES206. https://doi.org/10.1175/BAMS-D-16-0148.1.

Bojinski, S., Verstraete, M., Peterson, T.C., Richter, C., Simmons, A., Zemp, M., 2014. The concept of essential climate variables in support of climate research, applications, and policy. Bull. Am. Meteorol. Soc. 95 (9), 1431–1443. https://doi.org/10.1175/BAMS-D-13-00047.1.

Bolinder, M.A., Janzen, H.H., Gregorich, E.G., Angers, D.A., Vandenbygaart, A.J., 2007. An approach for estimating net primary productivity and annual carbon inputs to soil for common agricultural crops in Canada. Agric. Ecosyst. Environ. 118, 29–42. https://doi.org/10.1016/j.agee.2006.05.013.

Cao, J., Leng, G., Yang, P., Zhou, Q., Wu, W., 2022. Variability in crop response to spatiotemporal variation in climate in China, 1980–2014. Land 11 (8). https://doi.org/10.3390/land11081152.

Cardil, A., Rodrigues, M., Tapia, M., Barbero, R., Ramírez, J., Stoof, C.R., Silva, C.A., Mohan, M., de-Miguel, S., 2023. Climate teleconnections modulate global burned area. Nat. Commun. 14 (1), 1–10. https://doi.org/10.1038/s41467-023-36052-8.

Carr, M.K.V. (2001). The water relations and irrigation requirements of coffee. Experimental Agiculture, May. https://doi.org/10.1017/S0014479701001090.

Devasthale, A., Carlund, T., 2022. Recent trends in the agrometeorological climate variables over Scandinavia. Agric. For. Meteorol. 316 (January). https://doi.org/10.1016/j.agrformet.2022.108849.

Dikbaş, F., 2017. A novel two-dimensional correlation coefficient for assessing associations in time series data. Int. J. Climatol. 37 (11), 4065–4076. https://doi.org/10.1002/joc.4998.

Dommenget, D., Latif, M., 2002. A cautionary note on the interpretation of EOFs. J. Clim. 15 (2), 216–225. https://doi.org/10.1175/1520-0442(2002)015< 0216:ACNOTI> 2.0.CO;2.

Drápela, K., Drápelová, I., 2011. Appl. Mann-Kendall Test. Sen. " S. Slope Estim. Trend Detect. Depos. Data Bílý K. říž 1997 – 2010 4 (2), 133–146.

Droogers, P., Nkurunziza, P., Bastiaanssen, W.G.M., Immerzeel, W.W., Terink, W., Hunink, J.E., Meijninger, W., Hellegers, P., Chevalking, S., Steenbergen, F., & Brandsma, J.B. (2012). Assessment of the Irrigation Potential in South Sudan, Tanzania and Uganda: Vol. FutureWate (Issue 0).

Egonyu, J.P., Kagezi, G.K., Kucel, P., Ahumuza, G., Ogari, I., 2014. Phenology and Infestation Pattern of the Coffee Twig Borer, Xylosandrus compactus. ASIC 25th Int. Conf. Coffee Sci. 42–46.

Fang, X., Zhu, Q., Ren, L., Chen, H., Wang, K., Peng, C., 2018. Large-scale detection of vegetation dynamics and their potential drivers using MODIS images and BFAST: a case study in Quebec, Canada. Remote Sens. Environ. 206 (2016), 391–402.

Feddema, J.J., 2005. A revised thornthwaite-type global climate classification. Phys. Geogr. 26 (6), 442–466. https://doi.org/10.2747/0272-3646.26.6.442.

Funk, C., Rowland, J., Eilerts, G., White, L., 2012. A climate trend analysis of Uganda. Famine Early Warning Systems Network-Informing Climate Change Adaptation Series. Fact. Sheet 2012–3062, 1–4.

Gaona, J., Quintana-Seguí, P., Escorihuela, M.J., Boone, A., Llasat, M.C., 2022. Interactions between precipitation, evapotranspiration and soil-moisture-based indices to characterize drought with high-resolution remote sensing and land-surface model data. Nat. Hazards Earth Syst. Sci. 22 (10), 3461–3485. https://doi.org/10.5194/nhess-22-3461-2022.

Gebrechorkos, S.H., Hülsmann, S., Bernhofer, C., 2019. Long-term trends in rainfall and temperature using high-resolution climate datasets in East Africa. Sci. Rep. 9 (1), 1–9. https://doi.org/10.1038/s41598-019-47933-8.

Gobron, N., Pinty, B., Mélin, F., Taberner, M., Verstraete, M.M., Belward, A., Lavergne, T., Widlowski, J.L., 2005. The state of vegetation in Europe following the 2003 drought. Int. J. Remote Sens. 26 (9), 2013–2020. https://doi.org/10.1080/01431160412331330293.

Greene, C.A., Thirumalai, K., Kearney, K.A., Delgado, J.M., Schwanghart, W., Wolfenbarger, N.S., Thyng, K.M., Gwyther, D.E., Gardner, A.S., Blankenship, D.D., 2019. The climate data toolbox for MATLAB. Geochem., Geophys. Geosyst. 20 (7), 3774–3781. https://doi.org/10.1029/2019GC008392.

Grossiord, C., Buckley, T.N., Cernusak, L.A., Novick, K.A., Poulter, B., Siegwolf, R.T.W., Sperry, J.S., McDowell, N.G., 2020. Plant responses to rising vapor pressure deficit. N. Phytol. 226 (6), 1550–1566. https://doi.org/10.1111/nph.16485.

Gutierrez, M.V., Meinzer, F.C., 1994. Estimating water use and irrigation requirements of coffee in Hawaii. J. Am. Soc. Hortic. Sci. 119 (3), 652–657. https://doi.org/10.21273/jashs.119.3.652.

Hargreaves, George H., Samani, Zohrab A., 1985. Reference crop evapotranspiration from temperature. Appl. Eng. Agric. 1 (2), 96–99. https://doi.org/10.13031/2013.26773.

Harrington, P. de B., Urbas, A., Tandler, P.J., 2000. Two-dimensional correlation analysis. Chemom. Intell. Lab. Syst. 50 (2), 149–174. https://doi.org/10.1016/S0169-7439(99)00062-3.

Hunsaker, D.J., Pinter, P.J., Barnes, E.M., Kimball, B.A., 2003. Estimating cotton evapotranspiration crop coefficients with a multispectral vegetation index. Irrig. Sci. 22 (2), 95–104. https://doi.org/10.1007/s00271-003-0074-6.

Jensen, D.M., Burman, D.R., & Allen, R.G. (1990). Evapotranspiration and irrigation water requirements: a manual. In ASCE manuals and reports on engineering practice (USA). no. 70.

Kagezi, G., Kucel, P., Nakibuule, L., Kobusinge, J., Katondi, A.P., 2020. Field-based evidence of the black coffee twig borer infesting maesopsis eminii in coffee agro-systems in Kiboga District, Uganda. Uganda J. Agric. Sci. 19 (1), 15–20. https://doi.org/10.4314/ujas.v19i1.2.

Kagezi, G.H., Sseruyange, J., Kucel, P., Kobusinge, J., Nakibuule, L., Kabole, C., Wagoire, W.W., 2017. Fusarium spp. Associated with Xylosandrus compactus causing wilting in cocoa. J. Plant Pathol. 99 (2), 542. https://doi.org/10.4454/jpp.v99i2.3901.

Kansiime, M., Mulema, J., Karanja, D., Romney, D., & Day, R. (2017). Crop Pests and Disease Management in Uganda: Status and Investment Needs (Issue March).

Kath, J., Craparo, A., Fong, Y., Mittahalli Byrareddy, V., Davis, A., King, R., Nguyen-Huy, T., Van Asten, P.J.A., Marcussen, T., Mushtaq, S., Stone, R., Power, S., 2022. Vapour pressure deficit determines critical thresholds for global coffee production under climate change. Nat. Food 3. https://doi.org/10.1038/s43016-022-00614-8.

Kilama Luwa, J., Bamutaze, Y., Majaliwa Mwanjalolo, J.G., Waiswa, D., Pilesjö, P., Mukengere, E.B., 2021. Impacts of land use and land cover change in response to different driving forces in Uganda: evidence from a review. Afr. Geogr. Rev. 40 (4), 378–394. https://doi.org/10.1080/19376812.2020.1832547.

Kiran, M., Amare, H., & Semu, A. (2020). NBI Technical Reports: Water Resources Management series Mapping land suitability for irrigation in the Nile Basin.

Kumar, A. (2024). SpatialCorr3(Varargin). MATLAB. ⟨https://www.mathworks.com/matlabcentral/fileexchange/65640-spatialcorr3-varargin⟩.

Kumar, J., Umesh, U.N., Singh, A.K.P., 2020. Derivation of crop coefficient model of wheat and maize using growing degree days to mitigate climatic variability. Int. J. Curr. Microbiol. Appl. Sci. 9 (10), 2915–2924. https://doi.org/10.20546/ijcmas.2020.910.351.

Kuule, D.A., Ssentongo, B., Magaya, P.J., Mwesigwa, G.Y., Okurut, I.T., Nyombi, K., Egeru, A., Tabuti, J.R.S., 2022. Land Use and land cover change dynamics and perceived drivers in rangeland areas in central Uganda. Land 11 (9). https://doi.org/10.3390/land11091402.

Li, J., Li, Z.L., Wu, H., You, N., 2022. Trend, seasonality, and abrupt change detection method for land surface temperature time-series analysis: evaluation and improvement. Remote Sens. Environ. 280, 113222. https://doi.org/10.1016/J.RSE.2022.113222.

Li, Zengpeng, Tan, Z., 2014. Comparing cropland net primary production estimates frominventory, a satellite-based model, and a process-based model in theMidwest of the United States. Ecol. Model. 277 (2014), 1–12.

Li, Zhi, Zheng, F.L., Liu, W.Z., 2012. Spatiotemporal characteristics of reference evapotranspiration during 1961-2009 and its projected changes during 2011-2099 on the Loess Plateau of China. Agric. For. Meteorol. 154–155, 147. https://doi.org/10.1016/j.agrformet.2011.10.019.

Lorenz, E.N., 1956. Empirical orthogonal functions and statistical weather prediction. Tech. Rep. Stat. Forecast Proj. Rep. 1 Dep. Meteorol. MIT 49 1. Issue Scientific Report No. 1, Statistical Forecasting Project, p. 52.

Luiza, M., Carelli, C., Fahl, J.I., Ramalho, J.D.C., 2006. Asp. Nitrogen Metab. Coffee Plants 18 (1), 9–21.

Maidment, Ross, Allan, R.P., Greatrex, H., & Rojas, O. (2013). Evaluation of satellite-based and model re-analysis rainfall estimates for Uganda. September. https://doi.org/10.1002/met.1283.

Maidment, R., Black, E., & Young, M. (2017). TARCAT V3.1. https://doi.org/10.17864/1947.112.
Majaliwa, J.G., Tenywa, M., Bamanya, D., Majagu, W., Isabirye, P., Nandozi, C., Nampijja, J., Musinguzi, P., Nimusiima, A., Luswata, K.C., K.P.C, R., Bonabana, J., Bagamba, F., Sebuliba, E., Azanga, E., Sridher, G., 2015. Charact. Hist. Seas. Annu. Rainfall Temp. Trends Sel. Climatol. Homog. Rainfall Zones Uganda 15 (4).
Messié, M., Chavez, F., 2011. Global modes of sea surface temperature variability in relation to regional climate indices. J. Clim. 24 (16), 4314–4331. https://doi.org/10.1175/2011JCLI3941.1.
Mestas-Nuñez, A.M., Enfield, D.B., 1999. Rotated global modes of non-ENSO sea surface temperature variability. J. Clim. 12 (9), 2734–2746. https://doi.org/10.1175/1520-0442(1999)012< 2734:RGMONE> 2.0.CO;2.
Ministry of Agriculure, F., 2001. Crop Coefficients for Use in Irrigation Scheduling (and F.-B. C). Water Conserv. Factsheet 577, 1–6.
Mohapatra, S., Weisshaar, J.C., 2018. Modified Pearson correlation coefficient for two-color imaging in spherocylindrical cells. BMC Bioinforma. 19 (1), 1–14. https://doi.org/10.1186/s12859-018-2444-3.
Montazar, A., Krueger, R., Corwin, D., Pourreza, A., Little, C., Rios, S., Snyder, R.L., 2020. Determination of actual evapotranspiration and crop coefficients of California date palms using the residual of energy balance approach. Water 12 (8). https://doi.org/10.3390/w12082253.
Mubialiwo, A., Onyutha, C., Abebe, A., 2020. Historical rainfall and evapotranspiration changes over mpologoma catchment in Uganda. Adv. Meteorol. 2020 (March 2010). https://doi.org/10.1155/2020/8870935.
Mubiru, D.N., Radeny, M., Kyazze, F.B., Zziwa, A., Lwasa, J., Kinyangi, J., Mungai, C., 2018. Climate trends, risks and coping strategies in smallholder farming systems in Uganda. Clim. Risk Manag. 22 (August), 4–21. https://doi.org/10.1016/j.crm.2018.08.004.
Mugume, I. (2018). Optimization of Numerical Models for Operational Weather (Issue August). MAKERERE UNIVERSITY.
Mulovhedzi, N.E., Araya, N.A., Mengistu, M.G., Fessehazion, M.K., du Plooy, C.P., Araya, H.T., van der Laan, M., 2020. Estimating evapotranspiration and determining crop coefficients of irrigated sweet potato (Ipomoea batatas) grown in a semi-arid climate. Agric. Water Manag. 233, 1–34. https://doi.org/10.1016/j.agwat.2020.106099.
Myneni, R.B., Williams, D.L., 1994. On the relationship between FAPAR and NDVI. Remote Sens. Environ. 49 (3), 200–211. https://doi.org/10.1016/0034-4257(94)90016-7.
Nandy, S., Saranya, M., Srinet, R., 2022. Spatio-temporal variability of water use efficiency and its drivers in major forest formations in India. Remote Sens. Environ. 269, 112791. https://doi.org/10.1016/j.rse.2021.112791.
Nantumbwe, C., Tenywa, M., 2016. 6. Spat. Tempo Chang. Land Use Cover Atari Catchment Mt Elgon slopes 113–129. https://doi.org/10.4000/books.africae.1238.
NASA. (2022). Application for Extracting and Exploring Analysis Ready Samples (Appears). ⟨https://appeears.earthdatacloud.nasa.gov/⟩.
NICHOLSON, S.E., KLOTTER, D., HARTMAN, A.T., 2021. Lake-effect rains over lake victoria and their association with mesoscale convective systems. J. Hydrometeorol. 22, 1353–1368. https://doi.org/10.1175/JHM-D-20-0244.1.
Nielsen, P., 2009. Coastal and estuarine processes. Coast. Estuar. Process. 1–360. https://doi.org/10.1142/7114.
Nilsson, E., Becker, P., Uvo, C.B., 2020. Drivers of abrupt and gradual changes in agricultural systems in Chad. Reg. Environ. Change 20 (3). https://doi.org/10.1007/s10113-020-01668-9.
Nimusiima, A., Basalirwa, C.P.K., Majaliwa, J.G.M., Otim-Nape, W., Okello-Onen, J., Rubaire-Akiiki, C., Konde-Lule, J., Ogwal-Byenek, S., 2013. Nature and dynamics of climate variability in the uganda cattle corridor. Afr. J. Environ. Sci. Technol. 7 (August), 770–782. https://doi.org/10.5897/AJEST2013.1435.
Nsubuga, F.N.W., Olwoch, J.M., de, Rautenbach, C.J.W., Botai, O.J., 2014. Analysis of mid-twentieth century rainfall trends and variability over southwestern Uganda. Theor. Appl. Climatol. 115 (1–2), 53–71. https://doi.org/10.1007/s00704-013-0864-6.
Obubu, J.P., Mengistou, S., Fetahi, T., Alamirew, T., Odong, R., Ekwacu, S., 2021. Recent climate change in the lake kyoga basin, Uganda: An analysis using short-term and long-term data with standardized precipitation and anomaly indexes. Climate 9 (12). https://doi.org/10.3390/cli9120179.
Olatinwo, R.O., Service, F., & Hoogenboom, G. (2013). Efficient Crop Protection. October 2017. https://doi.org/10.1016/B978-0-12-398529-3.00005-1.
Onyutha, C., Asiimwe, A., Muhwezi, L., Mubialiwo, A., 2021. Water availability trends across water management zones in Uganda. Atmos. Sci. Lett. 22 (10), 1–14. https://doi.org/10.1002/asl.1059.
Pereira, A.R., Camargo, M.B.P. de, Villa Nova, N.A., 2011. Coffee crop coefficient for precision irrigation based on leaf area index. Bragantia 70 (4), 946–951. https://doi.org/10.1590/s0006-87052011000400030.
Phillips, J.G., Mcintyre, B.D., 2000. ENSO and interannual rainfall variability in Uganda: implications for agricultural management. Int. J. Climatol. 0088 (February). https://doi.org/10.1002/(SICI)1097-0088(200002)20.
Platform, G.C. (2019). The Uganda coffee roadmap.
Prince, S.D., Haskett, J., Steininger, M., Strand, H., Wright, R., 2001. Net primary production of U. S. midwest croplands from agricultural harvest yield data. Ecol. Appl. 11 (4), 1194–1205. ⟨https://esajournals.onlinelibrary.wiley.com/doi/epdf/10.1890/1051-0761%282001%29011%5B1194%3ANPPOUS%5D2.0.CO%3B2⟩.
Running, S., Mu, Q., & Ming, Z. (2017). MOD16A2 MODIS/Terra net evapotranspiration 8-day L4 global 500m SIN grid V061. https://doi.org/10.5067/MODIS/MOD16A2.006.
Sagehorn, M., Johnsdorf, M., Kisker, J., Sylvester, S., Gruber, T., Schöne, B., 2023. Real-life relevant face perception is not captured by the N170 but reflected in later potentials: a comparison of 2D and virtual reality stimuli. Front. Psychol. 14 (March). https://doi.org/10.3389/fpsyg.2023.1050892.
Sankaran, A., Krzyszczak, J., Baranowski, P., Sindhu, A.D., Kumar, N.P., Jayaprakash, N. L., Thankamani, V., Ali, M., 2020. Multifractal cross correlation analysis of agro-meteorological datasets (Including reference evapotranspiration) of california, united states. Atmosphere 11 (10), 1–24. https://doi.org/10.3390/atmos11101116.
Santos, L.M., Ferraz, G.A.S., Diotto, A.V., Barbosa, B.D.S., Maciel, D.T., Andrade, M.T., Ferraz, P.F.P., Rossi, G., 2020. Coffee crop coefficient prediction as a function of biophysical variables identified from RGB UAS images. Agron. Res. 18 (2), 1463–1471. https://doi.org/10.15159/AR.20.100.
Sen, P.K., 1968. Estimates of the regression coefficient based on Kendall's Tau. J. Am. Stat. Assoc. 63 (324), 1379–1389. https://doi.org/10.1080/01621459.1968.10480934.
Shamshiri, R.R., Jones, J.W., Thorp, K.R., Ahmad, D., Man, H.C., Taheri, S., 2018. Review of optimum temperature, humidity, and vapour pressure deficit for microclimate evaluation and control in greenhouse cultivation of tomato: a review. Int. Agrophys. 32 (2), 287–302. https://doi.org/10.1515/intag-2017-0005.
Sseremba, G., Tongoona, P.B., Musoli, P., Saviour, J., Eleblu, Y., Melomey, L.D., Bitalo, D.N., Atwijukire, E., Mulindwa, J., Aryatwijuka, N., Muhumuza, E., Kobusinge, J., Magambo, B., Kagezi, G.H., Danquah, E.Y., Kizito, E.B., Kyalo, G., Iyamulemye, E., 2023. Viability Deficit Irrig. Pre-Expo. Adapt. Robusta Coffee Drought Stress 1–14.
Stanton, M.C., Adriko, M., Arinaitwe, M., Howell, A., Davies, J., Allison, G., LaCourse, E. J., Muheki, E., Kabatereine, N.B., Stothard, J.R., 2017. Intestinal schistosomiasis in Uganda at high altitude (>1400m): malacological and epidemiological surveys on Mount Elgon and in Fort Portal crater lakes reveal extra preventive chemotherapy needs. Infect. Dis. Poverty 6 (1), 1–10. https://doi.org/10.1186/s40249-017-0248-8.
Stegman, E.C., 1988. Corn crop curve comparisons for the central and Northern plains of the Us. Appl. Eng. Agric. 4 (3), 226–233.
Tabari, H., Marofi, S., Aeini, A., Hosseinzadeh, P., Mohammadi, K., 2011. Trend analysis of reference evapotranspiration in the western half of Iran (https://doi.org/). Agric. For. Meteorol. 152 (2), 128–136. https://doi.org/10.1016/j.agrformet.2010.09.009.
TAMSAT. (2022). TAMSAT African Rainfall Climatology and Time series. ⟨http://www.tamsat.org.uk⟩.
The MathWorks Inc. (2019). MATLAB (version: 9.6.0 (R2019a)). The MathWorks Inc. ⟨https://www.mathworks.com⟩.
Thornthwaite, C.W., & Mather, J.R. (1955). The water balance. In Publications in climatology TA - TT -. Drexel Institute of Technology, Laboratory of Climatology. https://doi.org/LK - ⟨https://worldcat.org/title/637882076⟩.
Titus, A., & Pereira, G.N. (2017). Water Use Efficiency for Robusta Coffee. EcoFriendly Coffee. ⟨https://ecofriendlycoffee.org/water-use-efficiency-robusta-coffee/⟩.
Trajkovic, S., 2007. Hargreaves versus Penman-Monteith. J. Irrig. Drain. Eng. 133 (1), 38–42.
Tran, D.N.L., Nguyen, T.D., Pham, T.T., Rañola, R.F., Nguyen, T.A., 2021. Improving irrigation water use efficiency of robusta coffee (Coffea canephora) production in lam dong province, vietnam. Sustainability 13 (12), 1–17. https://doi.org/10.3390/su13126603.
UBOS. (2018). Uganda Bureau Of Statistics Abstract.
UCDA. (2022). Fact Sheet. ⟨https://ugandacoffee.go.ug/fact-sheet⟩.
Uganda National Meteorological Authority. (2022). Applied Meteorology, Data and Climate Services Directorate. ⟨https://unma.go.ug/directorates/applied-meteorology-data-and-climate-services⟩.
Van Rossum, G., & Drake Jr, F.L. (2009). Python 3 reference manual. CreateSpace. ⟨https://docs.python.org/3/reference/⟩.
Villazón, M.F., & Willems, P. (2010). Filling Gaps and Daily Disaccumulation of Precipitation Data for Rainfall-runoff model. Proceedings of the 4th International Science Conference BALWOI 2010, Ohrid, Republic of Macedonia, 25-29th May 2010.
Voda, A.I., Sarpe, C.A., Voda, M., 2018. Methods of maximum discharge computation in ungauged river basins. Review of procedures in Romania. Geogr. Tech. 13 (1), 130–137. https://doi.org/10.21163/GT_2018.131.12.
Wamucii, C.N., Van Oel, P.R., Ligtenberg, A., Gathenya, J.M., Teuling, A.J., 2021. Land use and climate change effects on water yield from East African forested water towers. Hydrol. Earth Syst. Sci. 25 (11), 5641–5665. https://doi.org/10.5194/hess-25-5641-2021.
Wang, N., Jassogne, L., Asten, P.J.A., Van, Mukasa, D., Wanyama, I., Kagezi, G., Giller, K. E., 2015. Evaluating coffee yield gaps and important biotic, abiotic, and management factors limiting coffee production in Uganda. Eur. J. Agron. 63, 1–11. https://doi.org/10.1016/j.eja.2014.11.003.
Waqas, M., Thandar, P., Wangwongchai, A., Dechpichai, P., 2024. Smart Agricultural Technology Determination of crop water requirements and potential evapotranspiration for sustainable coffee farming in response to future climate change scenarios. Smart Agric. Technol. 8, 100435. https://doi.org/10.1016/j.atech.2024.100435.
WMO. (2017). Chapter 5: Statistical Methods for Analysing Datasets. In World Meteorological Organization. ⟨http://www.wmo.int/pages/prog/wcp/ccl/guide/documents/english/WMO_100_en-chap5.pdf⟩.
World Bank. (2018). Uganda Economic Update: Developing the Agri-Food system for Inclusive Economic Growth. November.
World Meteorological Organization, 2012. Agrometeorlogy of some Selected Crops: Sorghum. Guide to Agricultural Meteorological Practices, pp. 1–128. ⟨http://www.wamis.org/agm/gamp/GAMP_Chap10.pdf⟩.
Wratt, D.S., Tait, A., Griffiths, G., Espie, P., Jessen, M., Keys, J., Ladd, M., Lew, D., Lowther, W., Mitchell, N., Morton, J., Reid, J., Reid, S., Richardson, A., Sansom, J., Shankar, U., 2006. Climate for crops: Integrating climate data with information

about soils and crop requirements to reduce risks in agricultural decision-making. Meteorol. Appl. 13 (4), 305–315. https://doi.org/10.1017/S1350482706002416.
Yosef, G., Alpert, P., Price, C., Rotenberg, E., Yakir, D., 2017. Using EOF analysis over a large area for assessing the climate impact of small-scale afforestation in a semiarid region. J. Appl. Meteorol. Climatol. 56 (9), 2545–2559. https://doi.org/10.1175/JAMC-D-16-0253.1.
Yue, S., Wang, C., 2004. Mann-Kendall Test. Modif. Eff. Sample Size Detect Trend Ser. Correl. Hydrol. Ser. 201–218.
Zakeri, F., Mariethoz, G., 2021. A review of geostatistical simulation models applied to satellite remote sensing: methods and applications. Remote Sens. Environ. 259 (February), 112381. https://doi.org/10.1016/j.rse.2021.112381.
Zhao, K., Wulder, M.A., Hu, T., Bright, R., Wu, Q., Qin, H., Li, Y., Toman, E., Mallick, B., Zhang, X., Brown, M., 2019. Detecting change-point, trend, and seasonality in satellite time series data to track abrupt changes and nonlinear dynamics: a Bayesian ensemble algorithm. Remote Sens. Environ. 232 (April 2018), 111181. https://doi.org/10.1016/j.rse.2019.04.034.